Stable isotope and calcareous nannofossil assemblage record of the late Paleocene and early Eocene (Cicogna section)

Claudia Agnini[12*], David J. A. Spofforth[3], Gerald R. Dickens[4,5], Domenico Rio[1], Heiko Pälike[6], Jan Backman[5], Giovanni Muttoni[7,8], Edoardo Dallanave[9]

[1] Dipartimento di Geoscienze, Università di Padova, Padova, Italy.

[2] Istituto di Geoscienze e Georisorse- Padova, CNR, Padova, Italy

[3] Robertson - CGG GeoSpec, Llandudno, United Kingdom

[4] Department of Earth Sciences, Rice University, Houston, Texas, USA.

[5] Department of Geological Sciences, Stockholm University, Stockholm, Sweden

[6] MARUM, University of Bremen, Bremen, Germany

[7] Dipartimento di Scienze della Terra "Ardito Desio", Università Statale di Milano, Milano, Italy

[8] ALP – Alpine Laboratory of Paleomagnetism, Peveragno (CN), Italy

[9] Ludwig-Maximilians, Universität München, München, Germany

[*]Corresponding author: C. Agnini, Dipartimento di Geoscienze, Università di Padova, 35131 Italy. (claudia.agnini@unipd.it)

Abstract. We present records of stable carbon and oxygen isotopes, $CaCO_3$ content, and changes in calcareous nannofossil assemblages across an 81 m thick section of upper Paleocene-lower Eocene marine sedimentary rocks now exposed along the Cicogna Stream in northeast Italy. The studied stratigraphic section represents sediment accumulation in a bathyal hemipelagic setting from approximately 57.5 to 52.2 Ma, a multi-million-year time interval characterized by perturbations in the global carbon cycle and changes in calcareous nannofossil assemblages. The bulk carbonate $\delta^{13}C$ profile for the Cicogna section, once placed on a common time scale, resembles that at several other locations across the world, and includes both a long-term drop in $\delta^{13}C$, and multiple short-term carbon isotope excursions (CIEs). This precise correlation of widely separated $\delta^{13}C$ records in marine sequences results from temporal changes in the carbon composition of the exogenic carbon cycle. However, diagenesis has likely modified the $\delta^{13}C$ record at Cicogna, an interpretation supported by variations in bulk carbonate $\delta^{18}O$, which do not conform to expectations for a primary signal. The record of $CaCO_3$ content reflects a combination of carbonate dilution and dissolution, as also inferred at other sites. Our detailed documentation and statistical analysis of calcareous nannofossil assemblages show major differences before, during and after the Paleocene Eocene Thermal Maximum. Other CIEs in our lower Paleogene section do not exhibit such a distinctive change; instead, these events are sometimes characterized by variations restricted to a limited number of taxa and transient shifts in the relative abundance of primary assemblage components. Both long-lasting and short-lived modifications to calcareous nannofossil assemblages preferentially affected nannoliths or holococcoliths such as *Discoaster, Fasciculithus, Rhomboaster/Tribrachiatus, Spenolithus* and *Zygrhablithus*, which underwent distinct variations in abundance as well as permanent evolutionary changes in terms of appearances and disappearances. By contrast, placoliths such as *Coccolithus* and *Toweius*, which represent the main component of the assemblages, were characterized by a gradual decline in abundance over time. Comparisons of

detailed nannofossil assemblage records at the Cicogna section and at ODP Site 1262 support the idea that variations in the relative and absolute abundances, even some minor changes, were globally synchronous. An obvious link is through climate forcing and carbon cycling, although the linkages between variations in calcareous nannoplankton, changes in $\delta^{13}C$ records and oceanography will need additional work.

INDEX TERMS

Paleocene, Eocene, calcareous nannofossils, stable isotopes, paleoclimate, Tethys

1 INTRODUCTION

A remarkable interval of global warming occurred from the middle Paleocene to the early Eocene, between approximately 59 and 51 million years ago (Ma). This inference comes from a variety of proxies (Huber and Caballero, 2011; Hollis et al., 2012), including the stable oxygen isotope ($\delta^{18}O$) composition of benthic foraminifera (**Figure 1**). The precise timing of the long-term temperature rise remains somewhat unconstrained, because absolute ages across the early Eocene remain unsolidified. Throughout this work, we assume that the Option-1 (WO-1) time scale presented by Westerhold et al. (2008) is correct (**Table 1**), but acknowledge that an offset of ca 400 kyr may occur within the time interval of interest (Vandenberghe et al., 2012). Debate also surrounds the magnitude and distribution of the temperature warming. Earth's surface temperatures, at least at high latitudes and in the deep sea, seem to have risen by at least 6°C from ca. 59 to 51 Ma (Zachos et al., 2008; Bijl et al., 2009; Huber and Caballero, 2011; Hollis et al., 2012). Indeed, the latter date marks the acme of the Early Eocene Climatic Optimum (EECO), the warmest sustained time interval of the Cenozoic (Zachos et al., 2008; Cramer et al., 2009; Hollis et al., 2012). Such a rise in

69 temperature is not obvious at low latitudes with current data (Pearson et al., 2007; Huber et al.,
70 2011).

71 Somehow related to long-term global warming were a series of major perturbations in the
72 global carbon cycle, as clearly indicated by stable carbon isotope ($\delta^{13}C$) records in benthic
73 foraminifera (**Figure 1**) and bulk carbonate in numerous marine sediment sequences (Shackleton,
74 1986; Corfield, 1994; Cramer et al., 2003; Zachos et al., 2008; 2010; Westerhold et al., 2011; Slotnick
75 et al., 2012). An overall increase in $\delta^{13}C$ occurred through most of the Paleocene, which climaxed in
76 a Cenozoic high at ca. 57.5 Ma (Westerhold et al., 2011), commonly referred to as the Paleocene
77 carbon isotope maximum (PCIM). From this time, $\delta^{13}C$ generally decreased to ca. 52.5 Ma. However,
78 when examined at higher temporal resolution, multiple $\delta^{13}C$ records show several short-term (<200
79 kyr) negative carbon isotope excursions (CIEs) (Cramer et al., 2003; Lourens et al., 2005; Nicolo et
80 al., 2007; Agnini et al., 2009; Zachos et al., 2010; Slotnick et al., 2012). Some of these CIEs clearly
81 coincided with rapid warming (above references). The most prominent and most widely
82 documented example of these "hyperthermals" was the Paleocene-Eocene Thermal Maximum
83 (PETM) at ca. 55.5 Ma, but other apparently similar events occurred at ca. 53.7 Ma (H1 or Eocene
84 Thermal Maximum 2, ETM-2), and at ca. 52.5 Ma (K/X, sometimes called ETM-3).

85 The early Paleogene in general, and the hyperthermals in particular, have attracted
86 considerable geoscience research. On one level, this is because these time intervals represent a
87 range of possible past analogues for understanding the effects of global warming and massive
88 carbon emissions (cf. Keeling and Whorf, 2004; Zachos et al., 2008). On another level, this is because
89 the long-term and short-term temperature and carbon cycle perturbations provide new
90 perspectives for how systems on Earth's surface operate. The PCIM probably represents a
91 tremendous storage of ^{13}C-depleted carbon somewhere on Earth's shallow surface (Shackleton,
92 1986; Kurtz et al., 2003; Komar et al., 2013). In turn, the CIEs probably signify rapid and large inputs

of ^{13}C-depleted carbon into the ocean and atmosphere (Dickens et al., 1997; Lourens et al., 2005; Zeebe et al., 2009). The middle Paleocene through early Eocene shows us that Earth's climate and carbon reservoirs were extremely dynamic during past times of global warmth. However, the composition and whereabouts of large quantities of transferable ^{13}C-depleted carbon (e.g., seafloor methane, peat, permafrost) remain uncertain (above references). Indeed, it is not clear if and how the long-term and short-term carbon cycle perturbations were related to one another, or to Earth surface temperatures.

The above context presents a series of basic questions to the geoscience community. Two of these are the focus of our study: (1) What is the correct template for understanding carbon cycling during the early Paleogene? Major changes in fluxes of ^{13}C-depleted carbon to the ocean or atmosphere should give predictable and coherent signals in the δ^{13}C of carbon-bearing phases across Earth, as well as the distribution of carbonate dissolution on the seafloor. This is not yet established. For example, several recently published δ^{13}C records (Kirtland-Turner et al., 2014; Slotnick et al., 2015a; Payros et al., 2015) do not precisely correlate with those at other locations (Cramer et al., 2003; Zachos et al., 2010; Slotnick et al., 2012, 2015b), at least with available stratigraphy. (2) How did marine calcifying organisms respond to major early Paleogene perturbations in temperature and carbon cycling, both in terms of evolution and preservation? The prominent changes in temperature and carbon fluxes almost assuredly caused large variations in seawater pH and carbonate ion concentration (CO_3^{2-}) (Dickens et al., 1997; Zachos et al., 2005; Kump et al., 2009; Zeebe et al., 2009; Leon-Rodriguez and Dickens, 2010; ; Hönisch et al., 2012; Pälike et al., 2012), although the response should depend on location and carbon fluxes involved (Dickens, 2000; Zeebe and Westbroek, 2003; Komar et al., 2013). Such changes might also affect the ability of living organisms to calcify (Riebesell et al., 2000, 2008; Kleypas et al., 2006; Iglesias-Rodriguez et al.,

2008; Stillman and Paganini, 2015), which might impact the fossil record (Agnini et al., 2006; Raffi and De Bernardi, 2008; Erba et al., 2010; Hönisch et al., 2012).

In regards to both questions, calcareous nannoplankton are an obvious group of organisms to focus on. This is because they are a main component of open ocean primary production (Milliman, 1993; Winter et al., 1994; Rost and Riebesell, 2004), because they are the dominate the output of carbonate in the ocean (Ziveri et al., 1999; Hay, 2004), and because they exhibit marked changes in species composition from the middle Paleocene through the early Eocene (Romein, 1979; Aubry, 1998, Bown et al., 2004; Gibbs et al., 2012). While numerous studies have examined calcareous nannofossils across the PETM from different perspectives (e.g., Bralower, 2002; Stoll and Bains, 2003; Gibbs et al., 2006a; 2006b; Agnini et al., 2007a; Mutterlose et al. 2007; Bown and Pearson, 2009; Jiang and Wise, 2009, Self-Trail et al., 2012), the relationship between these organisms and carbon cycle perturbations before and after this short-lived warming episode remain poorly documented (Gibbs et al., 2012). It seems possible that the high rate of calcareous nannofossil taxonomic evolution (appearances and extinctions), as well as distinct changes in calcareous nannofossil abundance patterns may provide excellent stratigraphic control across the early Paleogene (Bukry, 1973; Perch-Nielsen, 1985; Backman, 1986, Agnini et al., 2014). Moreover, if the exact relationship between changes in nannofossil assemblages and global carbon cycle perturbations were known, key time intervals could be rapidly identified for more detailed work. Finally, changes in calcareous nannofossils across the early Paleogene provide insights about the response of an important part of the sediment forming marine biota to changes in climate and carbon cycling.

Very few stratigraphic sections presently have detailed and coupled records of stable isotopes, carbonate content, and calcareous nannofossil abundances across the broad late Paleocene-early Eocene interval. The two notable exeptions are Ocean Drilling Program (ODP) Site 1262 (southeast

Atlantic) (Agnini et al., 2007b; Zachos et al., 2010) and Deep Sea Drilling Project (DSDP) Site 577 (northwest Pacific) (Shackleton, 1986; Dickens and Backman, 2013) (**Figure 2**). Here we present geochemical records ($\delta^{13}C$, $\delta^{18}O$ and $CaCO_3$ content) and calcareous nannofossil census data from the Cicogna section in northeast Italy (**Figures 2, 3**). These data are compared with similar information from Sites 1262 and 577. We show that the Cicogna section provides an important template for understanding potential relationships between climate, carbon cycling and the biotic evolution of calcareous nannoplankton.

2 THE CICOGNA SECTION

The Cicogna section crops out along the Cicogna Stream near the village of Tassei in the Belluno Province, northeast Italy (**Figure 3**). From a regional geological perspective, the sedimentary rocks of this section belong to the Belluno Basin. This basin represents part of a paleogeographic domain that formed when Jurassic rifting created a series of N–S oriented structural highs (platforms) and lows (basins), which persisted through much of the Paleogene (Bernoulli and Jenkyns, 1974; Bernoulli et al., 1979; Winterer and Bosellini, 1981). Importantly, from the Cretaceous to the middle-late Eocene, expanded deep sea sediment successions accumulated within the basins at nominally 30°N latitude (Stefani and Grandesso, 1991; Agnini et al., 2006; 2011; Zattin et al., 2006).

The Cicogna section consists of two lithostratigraphic units **(Figure 3**). The lower portion is a well-exposed upper Paleocene and lower Eocene unit referred to as Scaglia Rossa *sensu lato* (**Figures 3, 4**) (Giusberti et al., 2007; Dallanave et al., 2009). Based on benthic foraminiferal assemblages, the early Paleogene marls of this unit represent lithified pelagic and hemipelagic sediment that accumulated at middle to lower bathyal water depth, likely between 600 m and 1000 m and not deeper than 1500 m (Giusberti et al., 2007; 2015). The upper portion is a thick early to middle

164 Eocene unit called the Belluno Flysch (**Figures 3, 4**). This unit represents a synorogenic deposit on
165 the flanks of the former Trento and Friuli platforms (Grandesso, 1976; Doglioni and Bosellini, 1987).
166 Once corrected for bed strike and dip (ca. 315°N; ca. 45°) and bends in the stream, the Scaglia
167 Rossa at Cicogna measures 80 m in terms of stratigraphic height (Dallanave et al., 2009). The Belluno
168 Flysch measures 1 m in the Cicogna section. Furthermore, the section of interest can be subdivided
169 into several subunits (**Figure 4**). The lower 20 m is comprised of distinctive alternating beds of gray-
170 greenish to purple marls and calcareous marls, the latter defined by carbonate contents higher than
171 60% (**Figure 3c**). This is overlain by approximately 9 m of pink-red marls with much less lithologic
172 alternation. At 28.7 m, the sedimentary package is broken sharply by an approximately 3 m thick
173 red to brownish-red interval of clayey marls with sporadic grey-green cm-scale spots and lenses
174 (**Figure 3f, g**). This has been called the Clay Marl Unit (CMU), and records the core of the prominent
175 negative $\delta^{13}C$ excursion associated with the PETM at multiple outcrop sites within the Belluno Basin
176 (Agnini et al., 2006; 2007a; Giusberti et al., 2007). Above the CMU, from 31.7 to 39.2 m, the section
177 continues with deposition of rhythmic alternations of marls and calcareous marls (**Figure 3g**). Above
178 this 8.5 m thick interval, at ca. 40.5 m, spatic calcite crystals occur. Generally, couplets of marl and
179 calcareous marl couplets become less evident from 40.5 m until 54 m, where such couplets reoccur
180 (**Figure 3d**). At 75.5 m, a thin calcarenitic bed is encountered, presaging the onset of the Belluno
181 Flysch. This turbidite is followed by a temporary return to hemipelagic sedimentation that ends at
182 80.6 m. Above, sedimentation of the Belluno Flysch begins in earnest (**Figures 3b, 4**).
183 The basic stratigraphy of the Scaglia Rossa in the Cicogna section, including both polarity chron
184 boundaries and key calcareous nannofossil biohorizons has been published (Giusberti et al., 2007;
185 Dallanave et al., 2009). The combined biomagnetostratigraphy indicates that the 81 m of interest
186 spans polarity Chron C25r to Chron 23r, and calcareous nannofossil biozones CP6 to CP10 (Okada
187 and Bukry, 1980) or CNP10 to CNE4 (Agnini et al., 2014). Thus, the section represents a 5.3 million

188 year (Myr) long time interval, from about 57.5 to 52.2 Ma on the W0-1 time scale. This also implies
189 an average sedimentation rate (SR) of ca. 15 m/myr. Although the deposition of hemipelagic
190 sediment might suggest relatively constant SRs over time, the PETM and possibly other
191 hyperthermal events in the Belluno Basin were characterized by higher SRs (Giusberti et al. 2007;
192 Agnini et al., 2009; Tipple et al., 2011; Krishnan et al., 2015).

193 The Scaglia Rossa at Cicogna appears to record fairly continuous sediment accumulation at
194 moderately high deposition rates. This is important because it affords longer time duration than
195 most shallow ocean sites, greater time resolution than most deep ocean sites (**Figure 2**), and an
196 overall different environmental setting. Many early Paleogene records, especially those from paleo-
197 shelf environments, such as in Egypt (e.g, Aubry and Salem, 2012) and New Jersey (Mixon and
198 Powars, 1994; Harris et al., 2010), or from early deep sea drilling expeditions, such as in the Indian
199 Ocean (Slotnick et al., 2015b), are discontinuous, either because of hiatuses or core gaps. Much of
200 the detailed work and current understanding of stable carbon isotope stratigraphy and calcareous
201 nannofossil variations across the broad early Paleogene, therefore, has come from deep-sea drilling
202 sites with multiple holes but slow sedimentation rates, although we note the work in Clarence
203 Valley, New Zealand (**Figure 2**), another area that contains several paleo-slope sections with
204 moderately high sedimentation rates (Nicolo et al., 2007; Slotnick et al., 2012, 2015b; Dallanave et
205 al., 2015). For the Cicogna section, detailed stable isotope and $CaCO_3$ records are currently lacking,
206 as well as detailed calcareous nannofossil assemblage information, which we present here.
207
208 ## 3 MATERIAL AND METHODS
209
210 ### 3.1 Samples
211

A total of 492 samples were chiseled from outcrops along the section. Samples were selected so as to be as fresh and unaltered as possible. This included chipping off weathered surfaces while in the field. Each sample was calibrated to height (**Figure 4**). Samples then were split, with one portion powdered in an agate ball mill, and subsequently freeze-dried.

3.2 Geochemistry

Each powdered samples was analyzed for bulk sediment stable isotope composition at the Stable Isotope Laboratory, University of Southampton, UK. A known mass (~80 μg) was placed into a headspace vial, dried overnight, and flushed with helium. 10 mL of 100 % phosphoric acid was added to each sample and allowed to react. The liberated CO_2 gas was measured using an EUROPA Scientific GEO 20-20 mass spectrometer fitted with a microCAPS for carbonate analysis. Results are reported in standard delta notation relative to Vienna Pee Dee Belemnite (VPDB). An in-house standard of Carrara Marble, calibrated to NBS-19 Limestone, was measured multiple times to evaluate accuracy and precision. The external analytical precision (1σ), based on these replicate analyses, was 0.028 ‰ for $\delta^{13}C$ and 0.057 ‰ for $\delta^{18}O$.

The amount of $CaCO_3$ in each sample was calculated from the beam height response during isotope mass spectrometer measurements (Spofforth et al., 2010). The liberated CO_2 gas, when squeezed up in the bellows, is measured and generates a current, the beam height. The pressure of CO_2 gas is directly proportional to the beam height and therefore the mass of carbonate in the sample. Over 100 samples of pure $CaCO_3$, with masses between 200 and 480 μg, were analyzed to establish a linear relationship between beam height and carbonate content ($CaCO_3 = mx + b$; R^2 = 0.94 - 0.99). Results were validated by analyzing 30 samples on a C-H-N-O elemental analyzer.

3.3 Calcareous nannofossils

The un-powdered sample split was examined for calcareous nannofossils. Raw sediments were processed to prepare standard smear slides (Bown and Young, 1998). To assess the reproducibility of our counting methods in every single sample, a pivotal sample was prepared 10 times by two different operators. Repeated counts of the identical sample performed by different analysts gave similar results (sd <2-5 %). Particle density estimates (Baccelle and Bosellini, 1965) were not carried out because samples have a high range in the terrigenous content (22 to 90 %). An increase or decrease of the silicoclastic component is mainly related to the major or minor efficiency of the chemical and mechanical weathering on land (Agnini et al., 2009). In the studied sediments, the variation in the amount of the terrigenous content through time has modified the density of the allochemic particle component. Consequently, calcareous nannofossil absolute abundances could not be estimated correctly using a homogeneous/constant particle density or by weighing the same amount of sediment for each smear slide. However, the scope of semi-quantitative counts performed in this study is to recognize the precise position of biostratigraphic biohorizons rather than use these data as a proxy of the paleoproductivity of taxa. Essentially, the identification of the appearance or disappearance of any given taxon is not affected by its stratigraphic abundance pattern, which obviously reduces the negative effect of the variable abundance of the silicoclastic component throughout the section. Samples were examined under a Zeiss light microscope at 1250× magnification. Calcareous nannofossils were determined using taxonomy proposed by Aubry (1984, 1988, 1989, 1990, 1999), Perch-Nielsen (1985) and Bown (2005).

A total of 200 samples were examined, providing an average time resolution of ca. 25 kyr. A preliminary qualitative estimate of the abundance and preservation state of calcareous nannofossil assemblages was performed for all samples. An initial large batch (185) was analyzed primarily to

provide biostratigraphic control for the Cicogna section, and the basic resultshave been presented by Dallanave et al. (2009). We re-checked and refined the positions of some biohorizons by examining 15 additional samples, primarily across some of the CIEs, such as B1/B2, PETM, H1 and H2, and K/X (Cramer et al., 2003). The calcareous nannofossil biostratigraphic schemes used by Dallanave et al. (2009) were those of Martini (1971) and Okada and Bukry (1980). The new zonal scheme of Agnini et al. (2014) is also used here. Biohorizon nomenclature follows that given by Agnini et al. (2014): Base (B), Base common (Bc), Top (T) and Top common (Tc).

Calcareous nannofossil biostratigraphic results are based on semi-quantitative analyses, which is based on counts of the number of specimens of selected taxa present in a prefixed area, 1 mm^2 or 3 long traverses (modified after Backman and Shackleton, 1983). Calcareous nannofossil paleoecological results are instead based on relative abundances of calcareous nannofossil taxa (percent of the total assemblage), calculated from counts of at least 300 specimens.

To capture changes in calcareous nannofossil assemblages we also use a statistical approach. Principal Component Analysis (PCA) was preferred to other methods, as for instance non-metric dimensional scaling (MDS) procedure for which a small number of axes are chosen prior to the analysis and the data are fitted to these dimensions (Hammer et al., 2001). However, non-metric MDS results were performed and are available as supplementary data (Figure S2).

Principal component analysis (PCA) was performed on the percentages of 15 subgroups using the statistical software package, PAST ver. 2.17c (Hammer et al., 2001). Such analysis is often used for examining paleontological data (e.g., Buccianti et al., 2006; Kucera and Malmgren, 1998; Watkins and Self-Trail, 1992; Thibault and Gardin, 2010; Marino et al., 2012; Bordiga et al., 2015), as it can point out hypothetical variables (components) that explain much of the variance in a multidimensional data set. The first principal component accounts for the most variability in any dataset examined. Each succeeding component has the highest variance possible relative to the

preceding components (Hammer et al., 2001). This method also increases the symmetry, homoscedasticity and linearity of the data set (Aitchison, 1986). The chosen subgroups were: *Chiasmolithus, Coccolithus, Ellipsolithus, Discoaster, Ericsonia, Fasciculithus, Girgisia, Octolithus, Prinsius, Sphenolithus, Toweius, Rhomboaster/Tribrachiatus, Zyghrablithus,* reworked forms, and "others".

4 RESULTS

4.1 Carbon isotopes

The bulk rock $\delta^{13}C$ record for the Cicogna section can be described, in a general sense, as a long-term decrease of approximately 3 ‰, punctuated by a series of negative CIEs (**Figure 4**). The most prominent low in $\delta^{13}C$ coincides with the CMU.

Previously established polarity chron boundaries and key calcareous nannofossil biohorizons at the Cicogna section (Dallanave et al., 2009) provide very good stratigraphic framework. Once placed onto a common time scale, in this case WO-1 (Westerhold et al., 2008), the $\delta^{13}C$ record at Cicogna is fairly similar to those generated using upper Paleocene and lower Eocene marine carbonate at other locations (Cramer et al., 2003; Zachos et al., 2010; Slotnick et al., 2012). This includes, for example, bulk carbonate $\delta^{13}C$ records at ODP Site 1262, and DSDP Site 577 (**Figure 5**) The relatively high $\delta^{13}C$ values near the base of the Cicogna section document the late stages of the PCIM, which was centered within C25r (**Figure 1**). The overall drop in $\delta^{13}C$ across the section marks the long-term global decrease in $\delta^{13}C$ that lasted through Chron C24n (**Figure 1**). The record contains multiple negative shifts in $\delta^{13}C$. There is, however, an intriguing difference: across the Cicogna section, the long-term 3 ‰ shift in bulk carbonate $\delta^{13}C$ values is generally offset from that in bulk carbonate $\delta^{13}C$ records at Sites 1262 and 577 by approximately -1 ‰.

The superimposed CIEs are considered to correspond to CIEs found in $\delta^{13}C$ records from elsewhere, some of which represent known or inferred hyperthermal events (Cramer et al., 2003; Lourens et al., 2005; Nicolo et al., 2007; Zachos et al., 2010; Slotnick et al., 2012). There are three pairs of CIEs below the CMU (**Figure 4**), and during the initial upper Paleocene long-term decline in $\delta^{13}C$. These correspond with the B1/B2, C1/C2 and D1/D2 CIEs documented by others (Cramer et al., 2003; Zachos et al., 2010). Notably, at Site 1262, the B1/B2 CIEs occur during middle C25n, and the C1/C2 CIEs occur at the start of C24r (**Figure 5**). The same is true at Cicogna. Interestingly, at Cicogna, the B2 and C2 CIEs show greater magnitudes than the B1 and C1 CIEs, and these paired excursions are more pronounced than at all other locations examined to date. An additional paired CIE occurs in the uppermost Paleocene (**Figure 4**). This may correlate to a fourth set of late Paleocene CIEs documented at Site 1262 (Zachos et al., 2010).

The lower Eocene portion of the $\delta^{13}C$ record at Cicogna (**Figure 4**) begins at the CMU, which marks the PETM (Giusberti et al., 2007; Dallanave et al., 2009). As at many locations, the PETM is characterized by a prominent negative CIE. The shift in $\delta^{13}C$ at Cicogna is approximately -2.5 ‰, a decrease that begins abruptly at 28.7 m and returns more gradually to near pre-excursion values by about 33 m. From approximately 33 to 54 m, the $\delta^{13}C$ curve shows a relatively smooth trend. At 54 m, a pair of CIEs begin, with the first pair having a magnitude of about 1.0 ‰. These are the H1/H2 events (Cramer et al., 2003), which occurred in the upper part of Chron C24r (Lourens et al, 2005; Zachos et al., 2010; Dickens and Backman, 2013; Dallanave et al., 2015). Above the H1/H2 CIEs, and within Chron C24n, are a series of smaller (0.4 to 0.6 ‰) CIEs. Those at approximately 60, 65 and 72 m, are correlated with the I1/I2, J and K/X events, respectively. In summary, the $\delta^{13}C$ record at Cicogna correlates with that at ODP Site 1262 (Zachos et al., 2010) and DSDP Site 577 (Dickens and Backman, 2013) (**Figure 5**), as well as at several other locations (Cramer et al., 2003; Slotnick et al.,

2012; 2015b). This is important because it enables comparison and discussion between widely separated sedimentary records within a firm temporal framework.

4.2 Oxygen isotopes

The $\delta^{18}O$ values range from -1.08 to -3.64 ‰ with a mean value of -1.96 ‰ and a standard deviation (1σ) of 0.50 ‰ (**Figure 4**). However, at the broad scale, $\delta^{18}O$ increases upsection, with Paleocene samples averaging -2.10 ‰ and Eocene samples averaging -1.89 ‰. This trend is noteworthy because $\delta^{18}O$ values should decrease upsection, if the composition of the $CaCO_3$ was principally reflecting rising global temperatures through the early Eocene. The 1σ of $\delta^{18}O$ values also increases upsection, being 0.33 ‰ across Paleocene samples and 0.56 ‰ across Eocene samples.

There is virtually no correlation (r^2 = 0.014; r=0.12) between $\delta^{18}O$ and $\delta^{13}C$ values across all samples (**Figure 6)**. However, most "short-term" CIEs do display deceases in $\delta^{18}O$ (**Figure 4**). An interval of anomalously low $\delta^{18}O$ values occurs from 39.9 m to 40.9 m, where the spatic calcite was observed.

4.3 Carbonate content

The $CaCO_3$ content varies between 9.4 and 77.7 % across the sample suite, with a mean value of 54.3 % and a 1σ of 8.2 % (**Figure 4**). Two important findings emerge from the $CaCO_3$ content record. First, from 39 m to 54 m, where we find limited variance in the $\delta^{13}C$ curve, $CaCO_3$ content averages 52.1 % with a 1σ of 4.9 %. Thus, while the average is similar to that calculated for the entire section, the standard deviation is much less. At Site 1262, the corresponding time interval is also characterized by limited variance in $\delta^{13}C$ values and carbonate contents, the latter inferred from the

355 abundance of Fe counts in XRF scans (Zachos et al., 2010). Second, across all samples, the $CaCO_3$
356 content co-varies somewhat (r=0.29) with $\delta^{13}C$ (**Figure 6**). This is because several lows in $CaCO_3$
357 content coincide with minima in $\delta^{13}C$, as is obvious for the B1/B2, PETM and H1/H2 events (**Figure**
358 **4**).
359
360 **4.4 Calcareous nannofossils**
361
362 Calcareous nannofossils are generally abundant, diverse, and moderately well preserved. The sole
363 exception is across a 10 cm interval from 28.75 to 28.85 m, which corresponds to the onset of the
364 CIE that marks the PETM. The three samples from this interval are virtually barren of calcareous
365 nannofossils.
366 Secondary overgrowth of calcite can partially or wholly blur species-specific morphological
367 features. Such diagenetic alteration, however, only marginally influences the relative, semi-
368 quantitative andabsolute abundance of calcareous nannofossil taxa (Toffanin et al., 2013). Calcite
369 dissolution, on the other hand, can significantly affect the relative abundances of various calcareous
370 nannofossils within a given volume of sediment. This is because the removal of more dissolution
371 susceptible taxa, such as *Toweius* and holococcoliths, necessarily increases the abundance of less
372 dissolution susceptible taxa, such as discoasters (Roth and Thierstein, 1972; Adelseck et al., 1973;
373 Roth, 1983; Bornemann and Mutterlose, 2008; Toffanin et al., 2013). In general, moderate to strong
374 calcite dissolution also decreases the total abundance of calcareous nannofossils within a given
375 volume of sediment (Adelseck et al., 1973; Toffanin et al., 2011). In the Cicogna section, calcite
376 overgrowth on discoasters is the prevalent process affecting calcareous nannofossil assemblages
377 (**Plate I**). Most assemblages display high abundances (>1000 specimens/mm^2) and a high diversity,
378 which include more fragile taxa. It follows that dissolution has not severely altered most

assemblages in samples from the Cicogna section. Rather, the calcareous nannofossil record is considered to represent a genuine paleoecological signal.

Nannofossil assemblages from the Cicogna section display several general trends (**Figures 7-9**). At the most basic level, there is a decrease in the total number of nannofossils (N/mm^2) with decreasing age. Paleocene samples average approximately 2600 specimens/mm^2, whereas Eocene samples above the H1/H2 events average approximately 1200 specimens/mm^2. This decrease in abundance broadly corresponds to a change in calcareous nannofossil composition, as supported through a series of additional observations at the Cicogna section (**Figures 7-9**):

- *Coccolithus* and *Toweius* constitute nearly half of the assemblages considering the entire section. However, these genera show a clear decrease in abundance upsection, with a mean value of 60 % in Paleocene samples and 35 % in Eocene samples;
- *Zyghrablithus bijugatus* shows a low mean value of approximately 4 % in the Paleocene, followed by a sharp increase in the basal part of the Eocene, and a mean value of approximately 25 % upsection in the Eocene. Hence, the abundance of this taxon expands on behalf of *Coccolithus* and *Toweius*;
- *Sphenolithus* decreases progressively during the Paleocene, suddenly disappears at the onset of the PETM, before returning to and exceeding pre-PETM values in the lower Eocene. Thus, the abundance of sphenoliths also expands on behalf of *Coccolithus* and *Toweius*;
- *Fasciculithus* shows a severe decline in abundance and species diversity at the onset of the PETM (28.70 m), leading up to their extinction at 34.73 m;
- *Octolithus* is rare throughout most of the studied section, but displays high abundances from approximately 14.7 m to 27.5 m in the upper Paleocene;
- *Discoaster* does not show any distinct change in abundance except for a single peak at the onset of the PETM;

- Several Cretaceous and early Paleocene species constitute minor reworked components throughout the section. Notably, the intervals marked by the PETM, H1/H2 and, to a lesser extent, B1/B2 CIEs are characterized by higher abundances of these reworked components;
- Representatives of placolith genera, such as *Prinsius, Ericsonia, Chiasmolithus* and *Girgisia*, are minor components of most samples. *Prinsius* displays a marked permanent decrease in abundance from a mean value of approximately 6 % to 2.5 % across the Paleocene/Eocene boundary. By contrast, *Ericsonia* does not show a prominent difference in abundance between Paleocene and Eocene assemblages, but increases in abundance during known and suspected hyperthermal events;
- The Calcareous Nannofossil Excursion Taxa (CNET), which include *Discoaster araneus* and the genus *Rhomboaster* are present during the CIE of the PETM. The evolution of the *Rhomboaster*/*Tribrachiatus* plexus started at the onset of the PETM, when *Rhomboaster* and *T. bramlettei* first appeared, and continued into the lower Eocene with the successive appearances of *T. contortus* and *T. orthostylus* (Raffi et al., 2005; Agnini et al., 2006; 2007b).

Beyond the above variations, evolutionary appearances and extinctions occur during the studied time interval (**Figures 7-9**). Most of these species belong to *Discoaster, Sphenolithus* and the *Rhomboaster/Tribrachiatus* lineage, and include *D. multiradiatus, D. diastypus, D. lodoensis, S. radians, S. anarrhopus, T. bramlettei, T. contortus* and *T. orthostylus*. The biohorizons defined using these species are exceptionally useful for biostratigraphy and, interestingly, often occur close to changes in $\delta^{13}C$.

All assemblage data were used for PCA analysis. This indicates that PC1 (41.3 %) and PC2 (14.7 %) together account for 56 % of the variance in the dataset. The PCA graph (**Figure 8; Figure S1 supporting material**) shows that samples can be easily subdivided into three subgroups. The first two populations of samples are distinguished because of their different positions along the x-axis

427 (PC1). The third population can be separated from the other two because of its different position
428 along the y-axis (PC2). The use of a different statistical procedure, as for instance MDS, does not
429 substantially change these results (**Figure S2**).
430
431 **5 DISCUSSION**
432
433 **5.1 Integrated stratigraphy and a carbon isotope template**
434
435 Polarity chron boundaries and calcareous nannofossil biohorizons (**Table 1; Figure 4**) provide a solid
436 stratigraphic framework for the Cicogna section. Calcareous nannofossil biohorizons, including
437 additional ones defined here, align in same stratigraphic order when compared to other locations,
438 such as ODP Site 1262 and DSDP Site 577 (**Table 1; Figure 11**). The Cicogna section represents
439 sediment accumulation between 57.5 and 52.2 Ma on the WO-1 time scale (Dallanave et al., 2009).
440 The average SR was ca.15.2 m/Myr, although this must have varied (**Figures 3, 11**). The CMU, which
441 marks the "core" of the PETM and ca. 80-100 kyr, showing a higher sedimentation rate than much
442 of the remaining record (Dallanave et al., 2009; Krishnan et al., 2015).
443 Once placed into the above stratigraphic framework, the bulk carbonate $\delta^{13}C$ profile
444 documented at Cicogna correlates well to that generated at ODP Site 1262 (**Figure 5**). In fact, it is
445 similar to $\delta^{13}C$ profiles generated at multiple locations (**Figure 2, Figure S4**), as long as records have
446 been properly calibrated in both the depth and time domains. This includes accounting for core
447 stretching and core gaps at scientific drilling sites, such as at DSDP Site 577 (Dickens and Backman,
448 2013), and accounting for changing strike and dip along land sections, such as done at Cicogna
449 (**Figure 3**). During late Paleocene and early Eocene times, the Cicogna section records the long-term
450 decrease in $\delta^{13}C$. Superimposed on this drop were multiple, often paired, negative CIEs. The PETM

451 definitively represents the most prominent CIE, but several other CIEs occurred before and after.
452 Importantly, the relative positions of polarity chron boundaries, key calcareous nannofossil
453 biohorizons and CIEs at Cicogna align well with those found at other locations (**Table 1**; **Figures 5,**
454 **11**).

455 A clearly recognizable $\delta^{13}C$ pattern spans the late Paleocene through the early Eocene at several
456 locations (Cramer et al., 2003; Nicolo et al., 2007; Galeotti et al., 2010; Zachos et al., 2010; Slotnick
457 et al., 2012, 2015b), although the total number of CIEs remains uncertain. At Cicogna, the problem
458 lies in the interval surrounding the K/X event, which broadly corresponds to the start of the EECO
459 (see discussion in Slotnick et al., 2012). We cannot confirm with our sample resolution whether a
460 series of short-term, small amplitude CIEs mark this time, an idea suggested from $\delta^{13}C$ records of
461 the Clarence Valley sections (Slotnick et al., 2012; 2015b). However, as at other locations, such as
462 Site 1262, no significant CIEs occurred within the 1.6 Myrs between the PETM and the H-1/ETM-2
463 event (**Figure 5**).

464 The time-correlative $\delta^{13}C$ template implies changes in the mean ocean $\delta^{13}C$ of dissolved
465 inorganic carbon (DIC). In turn, these compositional changes very likely represent variations in fluxes
466 of highly ^{13}C-depleted carbon to and from the ocean or atmosphere, such as changes in the release
467 and storage of organic carbon (Shackleton, 1986; Dickens et al., 1997; Kurtz et al., 2003; Deconto et
468 al., 2010; Komar et al., 2013). The $\delta^{13}C$ record at Cicogna offers no direct insight on the location of
469 this carbon (e.g., seafloor methane, permafrost, peat). However, it does support an important
470 concept: the magnitudes of given CIEs appear somewhat related to one another and to the long-
471 term $\delta^{13}C$ record. In particular, the PETM occurred about halfway between the long-term high and
472 low in $\delta^{13}C$, and heralded a relatively long time interval lacking CIEs. A generic explanation is that a
473 very large mass of ^{13}C-depleted carbon was injected from some organic reservoir into the ocean or
474 atmosphere during the PETM, and that the reservoir needed to recharge for considerable time

475 before the next injection (H-1/ETM-2) could occur (Dickens et al., 2003; Kurtz et al., 2003; Lunt et
476 al., 2011; Komar et al., 2013).

477 The overall -1 ‰ offset of the $\delta^{13}C$ curve between the records at Cicogna and at Sites 577 and
478 1262 (**Figure 5**) warrants brief discussion. It probably does not reflect wholesale diagenesis and
479 resetting of the primary signal at any of these sections. Otherwise, a recognizable correlative $\delta^{13}C$
480 record and well-preserved nannofossils (**Plate I**) would not be found at all three locations. In fact, it
481 is difficult to modify the original $\delta^{13}C$ composition of carbonate over appreciable distance (> than
482 several meters) in marine sedimentary sequences dominated by fine grained calcite, even those
483 now exposed on land as lithified rock, such as at Cicogna or in the Clarence Valley. This is because
484 the carbon water/rock ratio remains low, because almost all carbon exists in carbonate, and because
485 temperature minimally influences carbon isotope fractionation (Matter et al., 1977; Scholle and
486 Arthur, 1980; Frank et al., 1999). Instead, the offset in the $\delta^{13}C$ curves probably relates to differences
487 in the composition of the original carbonate, a concept that we return to later.

488 However, local dissolution and re-precipitation of carbonate definitely has occurred in the
489 Cicogna section. This can be observed in the overgrowths of secondary calcite on discoasters and
490 *Rhomboaster/Tribrachiatus* (**Plate I**). This process should dampen the original CIEs, because on the
491 meter-scale, dissolution and re-precipitation of carbonate would involve $\delta^{13}C$ gradients in the DIC
492 of surrounding pore water (Matter et al., 1977; Scholle and Arthur, 1980). This may explain, in part,
493 why the magnitude of early PaleogeneCIEs in bulk carbonate records are often muted relative to
494 those found in other carbon-bearing phases (Slotnick et al., 2015b).

495

496 **5.2 Oxygen isotopes and a problem recording past temperatures**

497

498 The $\delta^{18}O$ record at Cicogna is intriguing because many of the CIEs are characterized by negative
499 excursions but absolute values of $\delta^{18}O$ generally and unexpectedly increase upsection (**Figure 4**).
500 Similar results have been documented in bulk carbonate stable isotope records at other locations,
501 such as ODP Site 1215 (Leon-Rodriguez and Dickens, 2010) and Mead Stream (Slotnick et al., 2012).
502 Even the $\delta^{18}O$ record of bulk carbonate at Site 1262 shows minimal long-term change from the late
503 Paleocene to the early Eocene (Zachos et al., 2010), the time when high-latitude surface
504 temperatures and deep ocean temperatures presumably increased by 5-6 °C, and one might expect
505 a >1 ‰ decrease in the $\delta^{18}O$ of marine carbonate.

506 Like previous workers, we cannot discount the notion that temperatures at low and high
507 latitudes responded differently across the early Paleogene (Pearson et al., 2007; Huber and
508 Caballero, 2011). Unlike for carbon isotopes, however, local dissolution and re-precipitation of
509 carbonate should significantly impact the $\delta^{18}O$ of marine carbonate. This is because the oxygen
510 water/rock ratio would be high before lithification, and because temperature strongly influences
511 oxygen isotope fractionation (Matter et al., 1975; Scholle and Arthur, 1980; Frank et al., 1999). In
512 general, as calcite-rich sediments and surrounding pore water are buried to higher temperatures
513 along a geothermal gradient, local dissolution and re-precipitation of carbonate shifts carbonate
514 $\delta^{18}O$ to lower values (above references; Schrag et al., 1995). It is likely that, during sediment burial,
515 the bulk carbonate $\delta^{18}O$ records in many lower Paleogene sections, including at Cicogna, have been
516 modified. We suggest that a signal of surface ocean temperature changes remains in the Cicogna
517 section, which gives rise to short-term $\delta^{18}O$ excursions that coincide with CIEs and several known or
518 suspected hyperthermal events. However, the entire $\delta^{18}O$ record at this location likely has shifted
519 to more negative values preferentially with increasing burial depth and age. This partly explains the
520 observed relationship between bulk carbonate $\delta^{13}C$ and $\delta^{18}O$, which lies along a trajectory expected
521 for diagenesis (**Figure 6**). A potential test of this idea would be to show that the overgrowths on

522 nannofossils (**Plate I**) have a significantly lower $\delta^{18}O$ than the primary core carbonate of nannofossil
523 tests.
524
525 **5.3 Calcareous nannofossil assemblages within the context of correlative stable isotope records**
526
527 A detailed stable carbon isotope curve provides a powerful tool to place past changes in calcareous
528 nannofossil assemblages into a highly resolved framework. This is because, as implied above, truly
529 global changes in the $\delta^{13}C$ composition of the ocean should occur within the cycling time of carbon
530 through ocean, which is <2000 years at present-day and presumably for the entire Cenozoic
531 (Broecker and Peng, 1982; Shackleton, 1986; Dickens et al., 1997).
532 Across the study interval at Cicogna, several calcareous nannofossil taxa appear or disappear
533 (**Table 1**). Moreover, their abundances also change between these horizons (**Figures 7-9**). One might
534 hypothesize that these changes in nannofossil assemblages were related to the established (e.g.,
535 the PETM, H1/ETM-2 and K/X) and potential (e.g., the B1/B2, I1/I2) hyperthermal events that
536 occurred during the late Paleocene and early Eocene (**Figures 1, 5**). However, the timing between
537 recorded evolutionary appearances and extinctions of calcareous nannofossils and perturbations in
538 $\delta^{13}C$ are variable (**Figures 7-9**). For instance, several significant calcareous nannofossil changes
539 observed close to H1/H2 hyperthermals (e.g., B *T. othostylus*, B *S. radians*, B *S. villae*, Tc *D.*
540 *multiradiatus,* T *T. contortus*) predate these events. By contrast, several biotic changes observed
541 close to the B1/B2 CIEs (e.g., B *D. delicatus,* Tc *S. anarrhopus,* B *D. multiradiatus*, T *Ericsonia robusta*)
542 happened at the end of these events. The PETM seems to provide the only case when a negative
543 CIE precisely corresponds to major changes in calcareous nannofossil assemblages.
544 Profound changes in calcareous nannofossil assemblages occurred across the PETM in several
545 locations (**Figure 2**), both in terms of relative abundances and increases in origination and extinction

546 rates (Aubry, 1998; Bown et al., 2004; Raffi et al., 2005; Gibbs et al., 2006a; Agnini et al., 2007a; Self-
547 Trail et al., 2012). At Cicogna, the assemblages show remarkable, though mostly transient, relative
548 abundance variations across the PETM, including an increase in *Coccolithus*, a decrease in
549 *Zygrhablithus, Sphenolithus, Toweius* and *Prinsius*, and an extinction of most fasciculith species
550 (**Figure 8**). Not surprisingly, these changes are very similar to those in the Forada section, which is
551 also located in the Belluno Basin (Agnini et al., 2007a).

552 Although these changes in relative abundance of taxa alone represent a notable difference with
553 respect to background conditions, most of the changes are transient and/or local when compared
554 with other datasets (Bralower, 2002; Gibbs et al., 2006b; Agnini et al., 2007b; Angori et al., 2007;
555 Mutterlose et al., 2007). For instance, an increase in abundance of *Discoaster* and *Fasciculithus* was
556 reported for some of the PETM section studied (e.g., Bralower, 2002; Tremolada and Bralower,
557 2004; Raffi et al. 2009), but these assemblage variations were not observed in other sections (e.g.,
558 Gibbs et al. 2006; Agnini et al., 2007a; Self-Trail et al., 2012). The only global calcareous nannofossil
559 assemblage features of the PETM are represented by the evolutionary appearance of
560 *Rhomboaster/Tribrachiatus* lineage, the presence during the CIE of short-lived species such as
561 *Discoaster areneus*, and the disappearance of several species of fasciculiths (Raffi et al., 2005; Agnini
562 et al., 2007a).

563 While changes in calcareous nannoplankton assemblages during the PETM have been
564 investigated at high resolution at different locations (e.g., Bralower, 2002, Gibbs et al., 2006b; Agnini
565 et al. 2007a), the longer-term perspective in which such changes occurred during the early
566 Paleogene has remained uncertain (Gibbs et al., 2012). The record at Cicogna provides this
567 opportunity.

568 The PCA analysis of calcareous nannofossil census data (%) indicates that two principal
569 components (PC1 and PC2) account for most (56.0 %) of the variability in our 15 selected subgroups.

570 Such analysis also permits the studied samples to be subdivided into three populations (**Figure 10**).
571 The first two populations are distinguished because of a major difference along the x-axis
572 representing PC1, whereas the third population stands out because of a significant difference along
573 the y-axis representing PC2. Importantly, each of these three populations constitutes a
574 homogeneous group in the time domain: Group 1 includes all upper Paleocene samples (Paleocene
575 samples and B1/B2 events); Group 2 consists of almost all lower Eocene samples (Eocene samples,
576 H1/H2 events and K event); Group 3 comprises samples that span the PETM (both core and
577 recovery), and two samples that come from sediment deposited during the core of the H1 and B2
578 events (**Figure 10**). These results indicate that late Paleocene calcareous nannofossil assemblages
579 are statistically different in their composition from those of early Eocene samples. Moreover, the
580 calcareous nannofossil assemblages across the PETM, and the climax of the B2 and H1 events, are
581 statistically different from those of either the late Paleocene or the early Eocene.

582 The general shift in the relative abundance of placoliths (i.e., *Coccolithus, Toweius* and *Prinsius*),
583 the major component of the late Paleocene assemblages, to nannoliths/holococcoliths (i.e.,
584 *Sphenolithus* and *Zygrhablithus*), the major component of the early Eocene assemblages, largely
585 explains the PC1 component. By contrast, the dramatic shift toward negative values in the PC2
586 component during the PETM happens because of the increase of *Ericsonia* and reworking and the
587 presence of *Rhomboaster-Tribrachiatus* plexus. Presumably, this relates to peculiar
588 paleoenviromental conditions that developed during the event. One can hypothesize that this may
589 have been a major difference in the physicochemical parameters of sea surface waters, such as
590 higher temperatures, higher nutrient concentration or reduced carbonate saturation state.

591 Statistical analysis of our data from Cicogna does not highlight any prominent short-term
592 changes in calcareous nannofossil assemblages, other than across the PETM and perhaps the B2 and
593 H1 events. However, several biohorizons occur around the B1/B2 events. Specifically, these are the

Bc *Z. bijugatus*, the brief high abundance of *Octolithus* spp., the evolutionary onset of the *D. delicatus/D. multiradiatus* lineage, the presence of the short-ranged *E. robusta*, the final radiation of late Paleocene fasciculiths (i.e., *F. richardii* group, *F. hayi, F. lilianae, F. alanii*), and the Tc of *S. anarrhopus*. All these happened at Cicogna and at Site 1262 within Chron C25n (Agnini et al., 2007b; Dallanave et al., 2009; **Figure 11)**, which spanned only 0.54 Myr (Westerhold et al., 2008). These near-synchronous events are intriguing because while the various nannofossils represent only minor components of late Paleogene assemblages, they were destined to become either an abundant constituent of Eocene populations (e.g., *Z. bijugatus* and the *D. delicatus/D. multiradiatus* lineage), or extinct after having been a distinctive element of Paleocene assemblages (e.g. *Fasciculithus* spp. and *S. anarrhopus)*. Following the PCIM, the long-term increase in temperature and decrease in $\delta^{13}C$ (**Figure 1**) coincided with a series of minor changes in nannofossil assemblages, which subsequently became important, presumably for evolutionary reasons.

Similar to the late Paleocene, calcareous nannofossil assemblages after the PETM do not show major rearrangements of common taxa during the early Eocene. Instead, minor components of these assemblages exhibit a sequence of closely spaced biohorizons. The sequence of these biohorizons is: T *Fasciculithus,* B *D. diastypus*, B *T. contortus,* T *T. bramlettei*, Tc *D. multiradiatus,* T *T. contortus*, B *T. orthostylus,* B *S. radians,* T *D. multiradiatus,* B *D. lodoensis,* B *G. gammation* and Bc *D. lodoensis* (**Table 1**). Within the resolution of available paleomagnetic and $\delta^{13}C$ data, all these biohorizons are virtually synchronous between the Cicogna section and ODP Site 1262 (**Figure 11**). They also almost all occurred in near synchrony at Site 577 (Dickens and Backman, 2013), although the precise correlation remains uncertain, given problems with coring disturbance and subtleties in age models at this location.

Importantly, for stratigraphic purposes, the B and Bc of *D. lodoensis* are approximately coeval at all three locations and spaced apart by about 750 kyr. Unless one examines samples in detail, these two biohorizons can be confused and result in an erroneous assignment of early Eocene ages.

The evolutionary appearances and extinctions amongst early Eocene nannofossil assemblages may suggest the presence of uneven communities living in an extreme climate in which alterations of environmental conditions, even minor, might trigger evolutionary changes or prominent variations in abundances of a limited number of taxa that typically do not represent the dominant component of assemblages. explained possible explanation is a generally higher tolerance of cosmopolitan taxa to variations in environmental conditions (Boucot, 1975; Winter et al., 1994). In contrast, highly specialized taxa that are adapted to a particular ecological niche, may display greater sensitivity to modifications in the photic zone environment (MacArthur and Wilson, 1967; Pianka, 1970; Baumann et al., 2005).

In summary, several genera of calcareous nannofossils, such as *Rhomboaster, Tribrachiatus, Sphenolithus, Discoaster* and *Zygrhablithus* were, at least to some extent, affected during the late Paleocene-early Eocene transition, because they show an increased rate of taxonomic evolution (**Figure 11**). However these genera are all minor groups in terms of overall abundance, at least in most lower Paleogene sediment sequences, and they all belong to nannoliths and holococcoliths. It appears that these organisms were more sensitive to environmental changes than heterococcoliths, for example the cosmopolitan genera *Coccolithus* and *Toweius*.

5.4 Early Paleogene calcareous nannofossil evolution

Any comprehensive paleoenvironmental interpretation involving early Paleogene calcareous nannofossils remains tentative because many taxa, such as *Rhomboaster*/*Tribrachiatus*, *Discoaster,*

640 *Sphenolithus* and *Zygrhablithus*, are extinct. Still, some single species or species groups are
641 considered to be useful for reconstructions of paleoenvironmental conditions (Geisen et al., 2004).
642 With that viewpoint, and with an understanding of modern holococcolith/nannolith ecology and
643 classical biogeographical model, we provide a scenario regarding late Paleocene-early Eocene
644 calcareous nannofossil evolution.

645 Modern holococcolithophores have numerous tiny rhombohedral calcite crystallites, and are
646 considered as haploid stages of certain heterococcolithophores, which can live in just about any
647 marine photic zone environment, although higher abundances and diversity are typical in
648 oligotrophic settings (Billard and Inouye, 2004). The most common Paleogene holococcolith was
649 *Zygrhablithus bijugatus.* This taxon has been interpreted as a *K*-specialist more adapted to stable
650 environments and oligotrophic conditions (Aubry, 1998; Bralower, 2002; Tremolada and Bralower,
651 2004; Agnini et al., 2007a; Self-Trail et al., 2012). Nannolith is a term used to describe peculiar
652 morphotypes usually observed in association with coccoliths, but lacking the typical features of
653 heterococcoliths or holococcoliths. *Ceratolithus cristatus,* a modern nannolith, has been observed
654 on the same cell together with *Neosphaera coccolithomorpha* (Alcolber and Jordan, 1997),
655 suggesting that the nannolith stage (*C. cristatus*) corresponds to the holococcolith stage in other
656 taxa (Young et al., 2005). Paleogene nannoliths include taxa with peculiar morphologies such as
657 *Discoaster, Fasciculithus* and *Sphenolithus*. These genera often have been associated with warm
658 waters and oligotrophic environments and are almost unanimously interpreted as *K*-specialists (Haq
659 and Lohmann, 1976; Backman, 1986; Wei and Wise, 1990; Bralower, 2002; Gibbs et al., 2004; 2006a;
660 2006b; Agnini et al., 2007a). *K* specialists fluctuate at or near the carrying capacity (K) of the
661 environment in which they thrive (MacArthur and Wilson, 1967), and are usually characterized by
662 long individual life-cycles and low reproductive potential. The *K*-specialist strategy is advantageous
663 in highly stable, typically oligotrophic environments, which allows the evolution of stenotopy and

where organisms compete by specialization and habitat partitioning (Hallock, 1987; Premoli Silva and Sliter, 1999). The narrow range of adaptability to changes in habitat or ecological conditions stimulates a rapid speciation.

At present, it is commonly accepted that modern holococcoliths and nannoliths are not produced by autonomous organisms; rather, they are stages in the life cycle of coccolithophores., Moreover, the passage between the two stages may be triggered by environmental factors (Billard and Inouye, 2004).

Hence, though Paleogene holococcoliths/nannoliths have no direct descendants in present-day oceans, they may very well have shared similar physiological features and life cycles with modern taxa. Assuming this is the case, the increase in the relative abundance of holococcoliths and nannoliths at the expense of heterococcoliths as well as the higher rates of evolution shown by holococcoliths and nannoliths may suggest conditions in which highly specialized taxa could flourish and rapidly evolve. This scenario is consistent with the idea, based on laboratory and modern ocean data, that the calcareous nannoplankton response to environmental change is species or group specific rather than homogeneous across the entire assemblage (Riebesell et al., 2000; Langer et al., 2006; Iglesias-Rodriguez et al., 2008; Lohbeck et al., 2012). Variations in the thermal and chemical structure of photic zone waters may thus account for the observed changes in the early Paleogene calcareous nannofossil assemblages.

5.5 Carbon isotope of surface waters during the early Paleogene

Like at Cicogna, well-preserved calcareous nannofossils dominate bulk sediment carbonate contents of early Paleogene strata at Sites 577 and 1262 (Backman, 1986; Zachos et al., 2004; Dickens and Backman, 2013). Given that the nannofossil assemblages are fairly similar (**Figure 11**), a really basic

688 question returns: why is the overall early Paleogene bulk carbonate $\delta^{13}C$ record at Cicogna less by
689 approximately 1 ‰?
690 A variety of explanations for the $\delta^{13}C$ offset can be offered. For example, sediments at Cicogna had
691 greater amounts of organic matter, and during burial diagenesis, a fraction of this carbon was
692 consistently added so as to decrease the $\delta^{13}C$ of pore water DIC. We note, though, that C_{org} contents
693 (wt %) at the proximal Forada section generally have values less than 0.1 wt % (Giusberti et al.,
694 2007). Similar C_{org} contents are found at ODP Site 1262, where values range from 0.0 to 0.3 wt %
695 (Zachos et al., 2004).
696 A cursory examination of early Paleogene bulk carbonate $\delta^{13}C$ records from other sites of the
697 North Atlantic/western Tethys region (e.g., Sites 550 and 1051; **Figure 2**) shows a commonality:
698 these locations also display negative 0.5 to 1 ‰ offsets relative to correlative records at Sites 577
699 and 1262 (Cramer et al., 2003). The $\delta^{13}C$ of DIC in modern surface waters (<100 m) ranges by about
700 2 ‰, because of the differences in temperature, primary productivity and water mass mixing
701 (Kroopnick, 1985; Tagliabue and Bopp, 2008). Notably, however, gradients in $\delta^{13}C$ of surface water
702 DIC are gradual, such that large regions have fairly similar values. It is possible that bulk carbonate
703 $\delta^{13}C$ values in early Paleogene North Atlantic sections record lower values than locations near the
704 Equator or in southern latitudes because of past ocean circulation.
705
706 **6 SUMMARY AND CONCLUSIONS**
707
708 We generate records of bulk carbonate $\delta^{13}C$ and $\delta^{18}O$, $CaCO_3$ content and calcareous nannofossil
709 assemblages from the Cicogna section, a marine sedimentary succession that now crops out along
710 a stream in the Southern Alps of northeast Italy. The combined geochemical and calcareous
711 nannofossil results allow us to generate a detailed stratigraphy for the section, as well as to explore

712 relationships between stable isotope variations and nannofossil assemblages. Most lower
713 Paleogene sections examined to date lack such coupled data sets.

714 The $\delta^{13}C$ record and calcareous nannofossil assemblages show that the section spans ~5.3 Myr
715 of the late Paleocene and early Eocene interval, from 57.5 to 52.2 Ma on the WO-1 timescale. This
716 is consistent with previous paleomagnetic information and preliminary calcareous nannofossil
717 biostratigraphy (Dallanave et al., 2009), but provides a more detailed stratigraphic framework, one
718 appropriate for correlations to other locations around the world. In particular, the fairly well
719 resolved $\delta^{13}C$ record shows long-term and short variations that correspond to those found in several
720 other sections, including an established series of negative CIEs. The most prominent CIE marks the
721 PETM, while other less pronounced CIEs represent the H-1, K/X and other "events" documented
722 elsewhere. The $\delta^{13}C$ variations observed at Cicogna clearly reflect global changes in the fluxes of
723 carbon to and from the ocean and atmosphere.

724 PCA analysis of calcareous nannofossil assemblages shows three distinct sample clusters. Late
725 Paleocene and early Eocene assemblages were distinctly different from each other and from that of
726 the PETM. Indeed, the PETM, the most intense hyperthermal during the late Paleocene - early
727 Eocene, was characterized by a unique calcareous nannofossil assemblage composition. This
728 suggests that the brief episode of extreme warming permanently modified the composition of
729 calcareous nannoplankton through an increase in the rate of taxonomic evolution (Gibbs et al.,
730 2006a). Less prominent hyperthermal events do not show significant variations in the main
731 components of assemblages, but rather were characterized by a series of changes affecting a limited
732 number of rare taxa. These taxa may have been less tolerant to environmental changes in their
733 habitats.

734 More common taxa, essentially consisting of placoliths, such as the cosmopolitan *Coccolithus*
735 and *Toweius*, display a progressive long-term decrease interrupted by transient changes in their

736 relative abundance but virtually no extinction or origination events occur in these groups during the
737 pertinent time interval. Species belonging to nannoliths and holococcoliths (*Discoaster,*
738 *Fasciculithus, Rhomboaster/Tribrachiatus, Sphenolithus* and *Zygrhablithus*), generally show a higher
739 rate of evolution and a higher concentration of biohorizons close to $\delta^{13}C$ perturbations. In
740 conclusion, calcareous nannoplankton show a different response of the various components of the
741 assemblages, this is consistent with a species or taxonomic unit sensitivity of calcareous
742 phytoplankton to paleoenviromental perturbations. This evolutionary climate-forced model is
743 supported by data from ODP Site 1262, which demonstrate that these changes are global and
744 synchronous between middle latitudes in the western Tethys region and the South Atlantic.
745

746 **7 ACKNOWLEDGMENTS**

747 CA would like to thank Carlotta Betto for preparing smear slides for calcareous nannofossil
748 analyses. We also acknowledge valuable comments from the referees two anonymous reviewers.
749 Funding for this work came from several sources. Primary support came from a MIUR grant to CA,
750 ED and DR (PRIN 2010-2011 - prot. 2010X3PP8J_003. JB acknowledges support from the Swedish
751 Research Council. GRD received funding from a National Science Foundation (NSF) grant (NSF-
752 FESD-OCE-1338842).

8 FIGURE AND TABLE CAPTIONS

Figure 1. Middle Paleocene to middle Eocene (64 to 48 Ma) stable isotope ($\delta^{13}C$ and $\delta^{18}O$) records of benthic foraminifera from multiple locations (Zachos et al., 2008) placed on the Option 1 (W01) time scale of Westerhold et al. (2008). Also shown are positions of polarity chrons and calcareous nannofossil biozones for this time interval, both from the CP Biozone scheme (Okada and Bukry, 1980) and the CN Biozone scheme (Agnini et al., 2014). Various "events" are noted within this chronostratigraphic framework, including the Paleocene carbon isotope maximum (PCIM), the Paleocene-Eocene thermal maximum (PETM), the H-1/ETM-2 event, the K/X event, and the Early Eocene Climatic Optimum (EECO). To the right is the general lithologic column and magnetostratigraphy of the Cicogna section (Dallanave et al., 2009).

Figure 2. Paleogeographic map indicating approximate locations at 55 Ma for several key sites with detailed stable isotope records across the late Paleocene and early Eocene. These include (marked with black dots and star) the Cicogna section (NE Italy, this study), DSDP Site 577 (Shatsky Rise, Dickens and Backman, 2013), ODP Sites 1051 (Blake Nose, Ogg and Bardot, 2001), 1215 (central Pacific, Raffi et al., 2005), and 1262 (Walvis Ridge, Westerhold et al., 2008), and the Clarence Valley (CV) sections (New Zealand, Slotnick et al., 2015b). The grey areas represent plate fragments, while the black lines show present-day shorelines. Boxes next to site locations show average sedimentation rates from the base of Chron C25n to the base of Chron C23r (57.20 - 52.36 Ma). The base map is from http://www.odsn.de/odsn/services/paleomap/paleomap.html. Red triangles are locations where a decrease in diversity of *Fasciculithus* spp. has been documented near the PETM. Locations include the Clarence Valley sections, central Pacific (ODP Sites 1215, 1220, 1221), western Pacific (DSDP Site 577 and ODP Site 865), South Atlantic (Walvis Ridge, DSDP Site 527, ODP Sites 1262,1263-1267; Maud Rise, ODP Site 690), equatorial Atlantic (Ceara Rise, ODP Site 929, Demerara

777 Rise, ODP Sites 1259, 1260), northwestern Atlantic (New Jersey Margin land sections, ODP Site 1051,
778 IODP Site U1403, U1409), northeastern Atlantic (Bay of Biscay DSDP Sites 401, 549 and 550, Zumaya
779 land section), Indian Ocean (DSDP Site 213; ODP 672; Kerguelen Plateau, ODP Site 1135)(Backman,
780 1986; Aubry, 1999; Bralower, 2002; Dupuis et al., 2003; Tremolada and Bralower, 2004; Bralower
781 and Mutterlose, 1995; Monechi et al., 2000; Gibbs et al., 2004; Raffi et al., 2005; Agnini et al., 2007a;
782 Angori et al., 2007, Mutterlose et al., 2007; Jiang and Wise, 2009; Shamrock, 2010; Norris et al, 2014;
783 Dallanave et al., 2015).
784
785 **Figure 3**. The location and representative photographs of the Cicogna section in northeast Italy. (a)
786 Geographic map showing the main Late Cretaceous–early Paleogene paleogeographic domains of
787 the Italian Southern Alps (modified after Cati et al., 1989); (b) Geological map of the local area
788 (modified after Costa et al, 1996 indicating also the location of the Cicogna section (red asterisk); (c)
789 Alternating beds of Paleocene gray-green marls and calcareous marls (0-20 m); (d) The Scaglia Rossa
790 *sensu latu* overlain by the Belluno Flysch; (e) Marl/calcareous marl couplets in the lower Eocene
791 portion of the section (approximately 40.0-70.0 m); (f) The base of the Clay Marl Unit, which denotes
792 the onset of the PETM (approximately 28.7-29.3 m); (g) The brownish-red interval of clayey marls
793 with sporadic grey-green cm-scale spots and lenses, the CMU, overlain by prominent rhythmic
794 alternations of marls and calcareous marls (approximately 28.7-33.0 m).
795
796 **Figure 4.** The Cicogna section with records of bulk carbonate $\delta^{13}C$ and $\delta^{18}O$ data, and $CaCO_3$ content.
797 Calcareous nannofossil biostratigraphy (CP and NP biozones) and magnetostratigraphy are after
798 Dallanave et al. (2009), CN biozones are also reported. Orange and yellow bands mark major $\delta^{13}C$
799 excursions. Dashed lines indicate minor CIEs that have been labeled elsewhere (e.g., E1/E2, F and

800 G; Cramer et al., 2003), whereas dotted lines indicate minor changes in $\delta^{13}C$ that appear to occur
801 also at ODP Site 1262 (see also **Figure 5**).
802
803 **Figure 5.** Stratigraphic correlation between upper Paleocene and lower Eocene sections at Cicogna,
804 ODP Site 1262 (Zachos et al., 2010), and DSDP Site 577 (Cramer et al., 2003; Dickens and Backman,
805 2013). All three sites have independently derived nannofossil biohorizons, polarity chrons and $\delta^{13}C$
806 records, which account for subtle temporal offsets. . Color bands and symbols are the same as in
807 Figure 4. Note the missing record at Site 577 that corresponds with known core gaps.
808
809 **Figure 6.** Plots of (a) bulk carbonate $\delta^{13}C$ versus bulk oxygen$\delta^{18}O$, and (b) bulk carbonate $\delta^{13}C$ versus
810 $CaCO_3$ contentfor samples from the Cicogna section. The black arrow shows the expected effect of
811 burial diagenesis. . Note the clear distinction in $\delta^{13}C$ for Paleocene and Eocene samples, which
812 relates to a long-term decrease in $\delta^{13}C$ (**Figure 5**).
813
814 **Figure 7.** Relative (%) and semi-quantitative (N/mm^2) abundances of selected calcareous
815 nannofossil genera across the Cicogna section. Also shown are the lithostratigraphy,
816 magnetostratigraphy, biostratigraphy and carbon isotope ($\delta^{13}C$) stratigraphy at the Cicogna section
817 (**Figure 4**). Color bands and symbols are the same as in previous figures.
818
819 **Figure 8.** Relative (%) and semi-quantitative (N/mm^2) abundances of selected, mainly late
820 Paleocene, calcareous nannofossil taxa across the Cicogna section. Also shown are the
821 lithostratigraphy, magnetostratigraphy, biostratigraphy and carbon isotope ($\delta^{13}C$) stratigraphy at
822 the Cicogna section (**Figure 4**). Color bands and symbols are the same as in previous figures.

Figure 9. Relative (%) and semi-quantitative (N/mm^2) abundances of selected, mainly early Eocene, calcareous nannofossil taxa across the Cicogna section. Also shown are the lithostratigraphy, magnetostratigraphy, biostratigraphy and carbon isotope ($\delta^{13}C$) stratigraphy at the Cicogna section (**Figure 4**). Color bands and symbols are the same as in previous figures.

Figure 10. Principal Component Analysis (PCA) of calcareous nannofossil percentage data of the Cicogna section. Calcareous nannofossils are subdivided into 15 subgroups (*Chiasmolithus, Coccolithus, Ellipsolithus, Discoaster, Ericsonia, Fasciculithus, Girgisia, Octolithus, Prinsius, Sphenolithus, Toweius, Rhomboaster/Tribrachiatus, Zyghrablithus*, reworking, others). Scatter plot of percentage data of calcareous nannofossil taxa of samples from the Cicogna section in terms of the first and second component. Each sample is represented by a circle and labelled. Different colors serve to separate sub-sets of samples having the same age.

Figure 11. Comparison of $\delta^{13}C$ profiles and semi-quantitative abundance patterns of selected calcareous nannofossil taxa from the Cicogna section and ODP Site 1262. Calcareous nannofossil biohorizons from DSDP Site 577 are reported in the right part of the figure. Orange and yellow bands mark CIEs shown in previous figures.). Color bands and symbols are the same as in previous figures.

Plate I. Images of selected calcareous nannofossil taxa from samples of the Cicogna section. Scale bar 10µm.

1. *Discoaster lodoensis* Bramlette and Riedel, 1954. Parallel light. Parallel nicols. Sample CIC/07-492. **2-3.** *Girgisia gammation* (Bramlette Sullivan, 1961) Varol 1989. Crossed nicols. Sample CIC/07-437. **4-5.** *Chiphragmalithus calathus* Bramlette and Sullivan, 1961; 4.Parallel light; 5. Crossed nicols. Sample CIC/07-447. **6-7.** *Sphenolithus radians* Deflandre in Grassé, 1952. 6. Crossed nicols 0°; 7.

Crossed nicols 45°. Sample CIC/07-437. **8.** *Tribrachiatus orthostylus* Shamrai, 1963. Parallel light. Sample 208-1262A-11H- 1, 149. Sample CIC/07-447. **9-10.** *Tribrachiatus contortus* (Stradner 1958) Bukry 1972. Parallel light. Sample CIC/07-335. **11-13.** *Zyghrablithus bijugatus* (Deflandre in Deflandre and Fert, 1954) Deflandre, 1959. Crossed nicols. Sample CIC/07-437. **14.** *Discoaster salisburgensis* Stradner, 1961. Parallel light. Sample CIC/07-335. **15.** *Discoaster diastypus* Bramlette and Sullivan, 1961. Parallel light. Sample CIC/07-335. **16.** *Fasciculithus tympaniformis* Hay and Mohler in Hay et al. 1967. Crossed nicols. Sample CIC/07-335. **17.** *Octolithus multiplus* (Perch-Nielsen, 1973) Romein, 1979. Crossed nicols. Sample CIC/07-122. **18.** *Discoaster multiradiatus* Bramlette and Riedel 1954. Parallel light. Sample CIC/07-122. **19.** *Toweius pertusus* (Sullivan, 1965) Romein, 1979. Crossed nicols. Sample CIC/07-122. **20.** *Toweius occultatus* (Locker, 1967) Perch-Nielsen, 1971. Crossed nicols. Sample CIC/07-122. **21.** *Toweius eminens* (Bramlette and Sullivan, 1961) Perch-Nielsen, 1971. Crossed nicols. Sample CIC/07-029. **22.** *Toweius eminens* (Bramlette and Sullivan, 1961) Perch-Nielsen, 1971. Crossed nicols. Sample CIC/07-029. **23.** *Toweius eminens* (Bramlette and Sullivan, 1961) Perch-Nielsen, 1971. Crossed nicols. Sample CIC/07-122. **24.** *Prinsius bisulcus* (Stradner, 1963) Hay and Mohler, 1967. Crossed nicols. Sample CIC/07-029. **25.** *Ericsonia robusta* Bramlette and Sullivan 1961. Crossed nicols. Sample CIC/07-029. **26-27.** *Sphenolithus anarrhopus* Bukry and Bramlette, 1969. 24. Crossed nicols 0°; 25. Crossed nicols 45°. Sample CIC/07-029. **28-29.** *Zyghrablithus bijugatus* (Deflandre in Deflandre and Fert, 1954) Deflandre, 1959. Crossed nicols. Sample CIC/07-122. **30.** *Thoracosphaera saxea* (Stradner, 1961). Crossed nicols. Sample CIC/07-122.

Table 1. Stratigraphic heights and ages of polarity chron boundaries, key calcareous nannofossil datums, and CIEs at the Cicogna Section and ODP Site 1262.

9. SUPPLEMENTARY INFORMATION

S2. Additional information on statistical analysis

Nannofossil data from the Cicogna section (NE Italy) were subjected to statistical analysis using the program PAST.

For PCA analysis, we additionally provide the biplot and the loading graphs of Component 1 and Component 2 (**Figure S1**).

For non-metric multidimensional scaling (MDS) analysis, the species counts were combined to produce a matrix of 15 genera. A square root transformation, used to standardize the matrix, was chosen to minimize the influence of dominant taxa on the ordination (Schneider et al., 2011). Non-metric multidimensional scaling (MDS), using the Bray–Curtis distance metric (**Figure S2**) was applied in order to avoid assumptions as much as possible and guarantee the preservation of the relative differences between the samples (McCune and Grace, 2002).

References

Schneider L.J., Bralower, T.J., Kump, L.R.: Response of nannoplankton to early Eocene ocean destratification, Palaeogeogr., Palaeoclimatol., Palaeoecol., 310, 152-162, 2011.

McCune, B., Grace, J.B.: Analysis of Ecology Communities. MjM Software Design, Gleneden Beach, Oregon, 2002.

S2. Further explanation regarding biostratigraphic calcareous nannofossil counts

The high abundance, widespread distribution and rapid evolution of calcareous nannofossils make them one of the most powerful tool to date Cenozoic marine sediments. The use of semi-quantitative counting and the gathering of high resolved datasets greatly enhance their correlation potential (Backman et al., 2012; Agnini et al., 2014).

The methodology used in this study for samples of ODP Site 1262 is that proposed by Backman and Shackleton (1983), which consists in counting the number of calcareous nannofossils belonging to a specific taxon present in a prefixed area (1 mm^2). Because of significant dilution by terrigenous material in samples from the Cicogna section, we extended the study area to 9 mm^2. To further

appreciate the importance of semi-quantitative estimates and high-resolution sampling, we compare the Top *D. multiradiatus* and Base *D. lodoensis* as recorded from the Cicogna section, ODP Site 1262 and DSDP Site 550 (**FigureS3**). At Cicogna and ODP Site 1262, we provide detailed abundance patterns of these two taxa. *Discoaster multiradiatus* shows a first decrease in abundance preceding the H1 event and a definitive disappearance just before the onset of the I1 event. *Discoaster lodoensis* displays a first presence in the I1 event, which is followed by an interval of absence that eventually leads to its continuous and common presence close to the onset of the X event (**Figure S3**). Datasets from the Cicogna section and ODP Site 1262 allow a very detailed characterization of these two biohorizons and the recognition of peculiar features that are not present in the low-resolution qualitative biostratigraphic data available for DSDP Site 550. As a consequence, the stratigraphic position of Top *D. multiradiatus* and Base *D. lodoensis* at DSDP Site 550 are inaccurate. We hope that this simple exercise could serve to emphasize the crucial importance of producing high-resolution semi-quantitative data to obtain the most reliable biostratigraphic results.

References

Ali, J. and Hailwood, E.: Magnetostratigraphic (re)calibration of the Paleocene/Eocene boundary interval in Holes 550 and 549, Goban Spur, eastern North Atlantic, Earth Planet. Sci. Lett., 161, 201-213, 1998.

Agnini, C., Fornaciari, E., Raffi, I., Rio, D., Röhl, U., and Westerhold, T.: High-resolution nannofossil biochronology of middle Paleocene to early Eocene at ODP Site 1262: implications for calcareous nannoplankton evolution. Mar. Micropaleontol., 64, 215-248, doi:10.1016/j.marmicro.2007.05.003, 2007b.

Agnini, C., Fornaciari, E., Raffi, I., Catanzariti, R., Pälike, H., Backman, J., and Rio, D.: Biozonation and biochronology of Paleogene calcareous nannofossils from low and middle latitudes, Newslett. Stratigr., 47, 131-181, doi:10.1127/0078-0421/2014/0042, 2014.

Backman, J., Raffi, I., Rio, D., Fornaciari, E. and Pälike, H., 2012: Biozonation and biochronology of Miocene through Pleistocene calcareous nannofossils from low and middle latitudes, Newsl. Stratigr., 45, 221-244.

Cramer, B. S., Wright, J. D., Kent, D. V., and Aubry, M.-P.: Orbital climate forcing of $\delta^{13}C$ excursions in the late Paleocene–early Eocene (Chrons C24n–C25n), Paleoceanography, 18 (4), 1097, doi:10.1029/2003PA000909, 2003.

930 Dallanave, E., Agnini, C., Muttoni, G., and Rio, D.: Magneto-biostratigraphy of the Cicogna section
931 (Italy): implications for the late Paleocene-early Eocene time scale, Earth Planet. Sci. Lett., 285,
932 39-51, doi:10.1016/j.epsl.2009.05.033, 2009.
933 Müller, C.: Biostratigraphic and paleoenvironmental interpretation of the Goban Spur region based
934 on a study of calcareous nannoplankton, Deep Sea Drill. Project, Initial Rep., 80, 389-414,
935 1985.
936 Westerhold, T., Röhl, U., Raffi, I., Fornaciari, E., Monechi, S., Reale, V., Bowles, J., and Evans, H. F.:
937 Astronomical calibration of the Paleocene time, Palaeogeogr. Palaeoclimatol. Palaeoecol.,
938 257, 377-403, doi:10.1016/j.palaeo.2007.09.016, 2008.
939 Zachos, J. C., Kroon, D., Blum, P., et al.: Early Cenozoic Extreme Climates: The Walvis Ridge Transect,
940 Proc. Ocean Drill. Program, Initial Rep., 208 doi:10.2973/odp.proc.ir.208.2004, 2004.
941
942 **S3. Looking through "frosty glass": Comparison to records at ODP Site 690**

943 We have presented fairly detailed records of bulk carbonate $\delta^{13}C$ and quantified calcareous
944 nannofossil assemblages for the lower Paleogene section at Cicogna, and compared these records
945 with those at the only two locations with similar information. From this comparison, we suggest
946 that a very detailed template exists for the alignment of $\delta^{13}C$ records and calcareous nannofossil
947 assemblage counts across the early Paleogene **(Figure 11**), one with much higher resolution than
948 given in most previous work, and one most likely related to changes in past global carbon cycling,
949 oceanography, and calcareous nannoplankton evolution.

950 Significant variations in calcareous nannofossil abundances definitely happened at multiple
951 locations during the PETM (Bralower, 2002, and references noted in main text). However, it is by no
952 means clear whether such changes extended across the broader early Paleogene, nor how such
953 changes might compare to those across the PETM. One can certainly speculate that variations in
954 calcareous nannofossil abundance records and bulk carbonate $\delta^{13}C$ records might correlate in fine
955 temporal detail across widely distributed sites throughout the early Paleogene, given well-
956 established calcareous nannofossil biozone schemes (Martini, 1971; Okada and Bukry, 1980; Agnini
957 et al., 2014), and a growing appreciation of a very dynamic carbon cycle over this time interval.
958 Nonetheless, the generation of detailed and coupled multi-million year records for quantified
959 calcareous nannofossil abundances and bulk carbonate $\delta^{13}C$ perplexed one of the referees for this

960 paper, who insisted that we needed to make comparisons with existing work at ODP Site 690 and
961 to explain discrepancies.

962 The lower Paleogene record at Site 690 provides a very good example in which to highlight the
963 basic background and importance of our work. Three holes were drilled and cored at ODP Site 690
964 on Maud Rise (South Atlantic; Figure 1) in 1987 using the advanced piston corer (APC) (Barker et al.,
965 1988). Sediment recovery within each core was nearly 100 %, although some cores were shorter
966 than the full 9.7 m. However, most of the lower Paleogene sequence was retrieved in only one of
967 the holes, 690B (Barker et al., 1988). This is important, because m-scale gaps generally occur
968 between successive cores during APC operations (Ruddiman et al., 1987; Lisiecki and Herbert, 2007).
969 The early Paleogene section at Site 690 is, almost assuredly, incomplete, with "missing" portions at
970 each core break.

971 Sediment from Core 690B-19H has been the focus of numerous papers, as it contains the PETM
972 (Kennett and Stott, 1991; Bains et al., 1999; Bralower, 2002). However, correlating this core to the
973 surrounding sedimentary record at Site 690, and the latter to early Paleogene records at other
974 locations is problematic, at least with any detail. For example, using Hole 690B records, Cramer et
975 al. (2003) estimated that 1.4 Myr occurred between the PETM and the H-1 event. This is incorrect,
976 as the duration is close to 1.8 Myr (Westerhold et al., 2008). Beyond the aforementioned core gaps,
977 there are major issues with the paleomagnetic record of early Paleogene sediments in Hole 690B
978 (Ali et al., 2000). Indeed, Ali et al. (2000) recommend using calcareous nannofossil records for
979 correlation purposes of this interval.

980 Records of bulk carbonate $\delta^{13}C$ (Cramer et al., 2003) and calcareous nannofossil relative
981 abundances (Pospichal and Wise, 1990) have been generated using sediment at Hole 690B. When
982 coupled together (**Figure S4**), these records show similarities to those at Cicogna (**Figure 11**). There
983 is the long-term late Paleocene-early Eocene drop in $\delta^{13}C$ and several superimposed short-term

negative CIEs. There are also closely coeval changes in calcareous nannofossil abundances, such as the peak in *D. multiradiatus* across the C event, the subsequent peak in *Fasciculithus* spp., and the cross-over of *T. contortus* and *T. orthostylus* just before the H-1 event. One can also see the problem with examining nannofossils at low depth/time resolution and qualitatively. We suggest here a "frosty glass" hypothesis, where details of Earth system change in the distant past are blurred presently by poorly resolved stratigraphy. This includes basic problems with aligning sections in depth and time, as well as interpretable quantification of data at high spatial resolution. Despite the need for additional work at Site 690, we suggest that available records at this location support the template offered in the main text.

References

Agnini, C., Fornaciari, E., Raffi, I., Catanzariti, R., Pälike, H., Backman, J., and Rio, D.: Biozonation and biochronology of Paleogene calcareous nannofossils from low and middle latitudes, Newslett. Stratigr., 47, 131-181, doi:10.1127/0078-0421/2014/0042, 2014.

Ali, J. R., Kent, D. V., and Hailwood, E. A.: Magnetostratigraphic reinvestigation of the Palaeocene/Eocene boundary interval in Hole 690B, Maud Rise, Antarctica, Geophys. J. Int., 141 (3), 639-646, doi: 10.1046/j.1365-246X.2000.00109.x, 2000.

Bains, S., Corfield, R. M. and Norris R. D.: Mechanisms of climate warming at the end of the Paleocene, Science, 285, 724-727, 1999.

Barker, P.E, Kennett, J.P., et al.: Proc. ODP, Init. Repts., 113, 1-774, doi:10.2973/odp.proc.ir.113.1988, 1988.

Bralower, T. .J.: Evidence of surface water oligotrophy during the Paleocene–Eocene thermal maximum: nannofossil assemblage data from Ocean Drilling Program Site 690, Maud Rise, Weddell Sea, Paleoceanography, 17, 1029-1042, doi:10.1029/2001PA000662, 2002.

Cramer, B. S., Wright, J. D., Kent, D. V., and Aubry, M.-P.: Orbital climate forcing of $\delta^{13}C$ excursions in the late Paleocene-early Eocene (Chrons C24n–C25n), Paleoceanography, 18 (4), 1097, doi:10.1029/2003PA000909, 2003.

Kennett, J. P. and Stott, L. D.: Abrupt deep-sea warming, palaeoceanographic changes and benthic extinctions at the end of the Palaeocene, Nature 353, 225-229 doi:10.1038/353225a0, 1991.

Lisiecki, L. E., and Herbert, T. D.: Automated composite depth scale construction and estimates of sediment core extension, Paleoceanography, 22(4), PA4213, doi:10.1029/2006PA001401, 2007.

Martini, E.: Standard Tertiary and Quaternary calcareous nannoplankton zonation, in: Proceedings of the 2nd Planktonic Conference, 2, Tecnoscienza, Roma, 739-785, 1971.

Okada, H., and Bukry, D.: Supplementary modification and introduction of code numbers to the low-latitude coccolith biostratigraphic zonation (Bukry, 1973; 1975), Mar. Micropaleontol., 5, 321-325, doi:10.1016/0377-8398(80)90016-X, 1980.

Pospichal, J. J., and Wise Jr., S. W.: Paleocene to middle Eocene calcareous nannofossils of Maud Rise, Weddell Sea, Proc. Ocean Drill. Program, Sci. Results, 113, 613-638, doi:10.2973/odp.proc.sr.113.205.1990, 1990.

Ruddiman, W. F., Cameron, D., and Clement, B. M.: Sediment disturbance and correlation of offset holes drilled with the hydraulic piston corer, Proc. Deep Sea Drill. Project, Init. Repts., 94, 615–634. doi:10.2973/dsdp.proc.94.111.1987, 1987.
Westerhold, T., Röhl, U., Raffi, I., Fornaciari, E., Monechi, S., Reale, V., Bowles, J., and Evans, H. F.: Astronomical calibration of the Paleocene time, Palaeogeogr. Palaeoclimatol. Palaeoecol., 257, 377-403, doi:10.1016/j.palaeo.2007.09.016, 2008.

Supplementary figure captionsFigure S1. PCA plots of calcareous nannofossil data from the Cicogna section (Italy). A) Loading plot of Component 1; B) Loading plot of Component 2; C) Biplot.

Figure S2. Non-metric multidimensional scaling (NMS) plot of calcareous nannofossil data from the Cicogna section (Italy). Grey dots = barren to virtually barren samples.

Figure S3. Abundance patterns of *D. multiradiatus* and *D. lodoensis* from the Cicogna section, ODP Site 1262 and DSDP Site 550. For these three successions paleomagnetic (Ali and Hailwood, 1998; Dallanave et al., 2009; Westerhold et al., 2008), carbon isotope (Cramer et al., 2003; Zachos et al., 2004; this study) and calcareous nannofossil data (Müller, 1985; Agnini et al., 2007, this study) are available. Top *D. multiradiatus* and Base *D. lodoensis* are clearly recognizable at Cicogna and ODP Site 1262, where quantitative counts have been performed. By contrast, qualitative data from DSDP Site 550 do not provide reliable biostratigraphic data P= present; R=rare; F=few; C=common; A=abundant; V=very abundant.

Figure S4. Carbon isotope data from ODP Site 690 (Cramer et al., 2003) plotted against qualitative abundance estimates of selected calcareous nannofossil taxa (Pospichal and Wei, 1990). Top *Fasciculithus* spp. (Aubry et al., 1996)

Table S1. Bulk carbonate stable isotopes and carbonate content of samples from the Cicogna section.

Table S2. Calcareous nannofossil assemblage counts for samples from the Cicogna section.

Table S3. Dataset used to perform the principal component analysis for calcareous nannofossil assemblages from the Cicogna section. Calcareous nannofossils are subdivided in 15 subgroups

(*Chiasmolithus, Coccolithus, Ellipsolithus, Discoaster, Ericsonia, Fascicuithus, Girgisia, Octolithus, Prinsius, Sphenolithus, Toweius, Rhomboaster/Tribrachiatus, Zyghrablithus*, reworking, others). In order to avoid the closed-sum effect that derives from the use of percentage data, we apply a log transformation of raw data.

Table S4. Dataset used to perform the non-metric multidimensional scaling (MDS) for calcareous nannofossil assemblages from the Cicogna section. Calcareous nannofossils are subdivided in 15 subgroups (*Chiasmolithus, Coccolithus, Ellipsolithus, Discoaster, Ericsonia, Fascicuithus, Girgisia, Octolithus, Prinsius, Sphenolithus, Toweius, Rhomboaster/Tribrachiatus, Zyghrablithus*, reworking, others). A square root transformation was used to minimize the influence of dominant taxa on the ordination.

10 REFERENCES

Adelseck Jr., C. G., Geehan, G. W., and Roth, P. H.: Experimental evidence for the selective dissolution and overgrowth of calcareous nannofossils during diagenesis, Geol. Soc. Am. Bull., 84, 2755-2762, 1973.

Agnini, C., Muttoni, G., Kent, D. V., and Rio, D.: Eocene biostratigraphy and magnetic stratigraphy from Possagno, Italy: The calcareous nannofossil response to climate variability, Earth Planet. Sci. Lett., 241, 815-830, doi:10.1016/j.epsl.2005.11.005, 2006.

Agnini, C., Fornaciari, E., Rio, D., Tateo, F., Backman, J., and Giusberti, L.: Responses of calcareous nannofossil assemblages, mineralogy and geochemistry to the environmental perturbations across the Paleocene/Eocene boundary in the Venetian Pre–Alps, Mar. Micropaleontol., 63, 19-38, doi:10.1016/j.marmicro.2006.10.002, 2007a.

Agnini, C., Fornaciari, E., Raffi, I., Rio, D., Röhl, U., and Westerhold, T.: High-resolution nannofossil biochronology of middle Paleocene to early Eocene at ODP Site 1262: implications for calcareous nannoplankton evolution. Mar. Micropaleontol., 64, 215-248, doi:10.1016/j.marmicro.2007.05.003, 2007b.

Agnini, C., Macrì, P., Backman, J., Brinkhuis, H., Fornaciari, E., Giusberti, L., Luciani, V., Rio, D., Sluijs, A., and Speranza, F.: An early Eocene carbon cycle perturbation at 52.5 Ma in the Southern Alps: Chronology and biotic response, Paleoceanography, 24, PA2209, doi:10.1029/2008PA001649, 2009.

Agnini, C., Fornaciari, E., Giusberti, L., Grandesso, P., Lanci, L., Luciani, V., Muttoni, G., Pälike, H., Rio, D., Spofforth, D. J. A., and Stefani, C.: Integrated bio-magnetostratigraphy of the Alano section (NE Italy): a proposal for defining the middle-late Eocene boundary, Geol. Soc. Am. Bull., 123, 841-872, doi:10.1130/B30158.1, 2011.

Agnini, C., Fornaciari, E., Raffi, I., Catanzariti, R., Pälike, H., Backman, J., and Rio, D.: Biozonation and biochronology of Paleogene calcareous nannofossils from low and middle latitudes, Newslett. Stratigr., 47, 131-181, doi:10.1127/0078-0421/2014/0042, 2014.

Aitchison, J.: The Statistical Analysis of Compositional Data. Chapman and Hall, London - New York, 12, 1-416, 1986.

Alcober, J. A. and Jordan, R. W.: An interesting association between *Neosphaera coccolithomorpha* and *Ceratolithus cristatus,* Eur. J . Phycol, 32, 91-93, 1997.

Angori, E., Bernaola, G., and Monechi, S.: Calcareous nannofossil assemblages and their response to the Paleocene-Eocene Thermal Maximum event at different latitudes: ODP Site 690 and Tethyan sections, Geol. Soc. Am. Spec. Pap., 424, 69-85, doi:10.1130/2007.2424(04), 2007.

Aubry, M.-P.: Handbook of Cenozoic Calcareous Nannoplankton, book 1, Ortholithae (Discoaster), Am. Mus. Nat. Hist. Micropaleontol. Press, New York, 1-263, 1984.

Aubry, M.-P.: Handbook of Cenozoic Calcareous Nannoplankton, book 2, Ortholithae (Holococcoliths, Ceratoliths, Ortholiths and Other), Am. Mus. Nat. Hist. Micropaleontol. Press, New York, 1-279, 1988.

Aubry, M.-P.: Handbook of Cenozoic Calcareous Nannoplankton, book 3, Ortholithae (Pentaliths and Other), Heliolithae (Fasciculiths, Sphenoliths and Other), Am. Mus. Nat. Hist. Micropaleontol. Press, New York, 1-279, 1989.

Aubry, M.-P.: Handbook of Cenozoic Calcareous Nannoplankton, book 4, Heliolithae (Helicoliths, Cribriliths, Lopadoliths and Other), Am. Mus. Nat. Hist. Micropaleontol. Press, New York, 1-381, 1990.

Aubry, M.-P.: Early Paleogene calcareous nannoplankton evolution: a tale of climatic amelioration, in: Late Paleocene–early Eocene Biotic and Climatic Events in the Marine and Terrestrial Records, Columbia University Press, New York, 158-201, 1998.

Aubry, M.-P.: Handbook of Cenozoic Calcareous Nannoplankton, book 5, Heliolithae (Zygoliths and Rhabdoliths), Am. Mus. Nat. Hist. Micropaleontol. Press, New York, 1-368, 1999.

Aubry, M.-P.: Late Paleocene–early Eocene sedimentary history in western Cuba: implications for the LPTM and for regional tectonic history, Micropaleontol., 45, 5-18, 1999.

Aubry, M.-P. and Salem, R.: The Dababiya Core: A window into Paleocene to early Eocene depositional history in Egypt based on coccolith stratigraphy, Stratigraphy, 9, 287-346, 2012.

Baccelle, L. and Bosellini, A.: Diagrammi per la stima visiva della composizione percentuale nelle rocce sedimentary, Ann. Univ. Ferrara, 9, 4, 59-62, 1965.

Backman, J.: Late Paleocene to middle Eocene calcareous nannofossil biochronology from the Shatsky Rise, Walvis Ridge and Italy, Palaeogeogr. Palaeoclimatol. Palaeoecol., 57, 43-59, 1986.

Backman, J. and Shackleton N. J.: Quantitative biochronology of Pliocene and early Pleistocene calcareous nannoplankton from the Atlantic, Indian and Pacific Oceans, Mar. Micropaleontol., 8, 141-170, doi:10.1016/0377-8398(83)90009-9, 1983.

Baumann, K.-H., Andruleit, H., Böckel, B., Geisen, M., and Kinkel, H.: The significance of extant coccolithophores as indicators of ocean water masses, surface water temperature, and palaeoproductivity: a review, Paläontol. Zeitsch., 79, 93-112, 2005.

Bernoulli, D., and Jenkyns, H.C.: Alpine, Mediterranean, and Central Atlantic Mesozoic facies in relation to the early evolution of the Tethys, in: Modern and Ancient Geosynclinal Sedimentation, Society for Sedimentary Geology (SEPM) Special Publication, 19, 19–160, 1974.

Bernoulli, D., Caron, C., Homewood, P., Kalin, O., and Van Stuijvenberg, J.: Evolution of continental margins in the Alps, Schweiz. Miner. Petrog., 59, 165-170, 1979.

Bijl, P. K., Schouten, S., Sluijs, A., Reichart, G. J., Zachos, J. C., Brinkhuis, H.: Early Palaeogene temperature evolution of the southwest Pacific Ocean, Nature, 461, 776–779, doi:10.1038/nature08399, 2009.

Billard, C. and Innouye, I.: What is new in coccolithophore biology?, in: Coccolithophores - From Molecular Processes to Global Impact, Springer, Berlin, 1-29, 2004.

Bordiga, M., Henderiks, J., Tori, F., Monechi, S., Fenero, R., and Thomas, E.: The Eocene–Oligocene transition at ODP Site 1263, Atlantic Ocean: decreases in nannoplankton size and abundance and correlation with benthic foraminiferal assemblages, Clim. Past Discuss., 11, 1615-1664, doi:10.5194/cpd-11-1615-2015, 2015.

Bornemann, A. and Mutterlose, J.: Calcareous nannofossil and $\delta^{13}C$ records from the Early Cretaceous of the Western Atlantic Ocean: evidence for enhanced fertilization across the Berriasian–Valanginian transition, Palaios, 23, 821-832, 2008.

Boucot, A. J.: Evolution and Extinction Rate Controls. Elsevier, Amsterdam, The Netherlands, 250p. 1975.

Bown, P. R.: Paleogene calcareous nannofossils from the Kilwa and Lindi areas of coastal Tanzania: Tanzania Drilling Project Sites 1 to 10, J. Nannoplankt. Res., 27, 21-95, 2005.

Bown, P., and Pearson, P.: Calcareous plankton evolution and the Paleocene/Eocene thermal maximum event: New evidence from Tanzania, Mar. Micropaleontol., 71, 60-70, doi: 10.1016/j.marmicro.2009.01.005, 2009.

Bown, P. R. and Young, J. R.: Techniques, in: Calcareous Nannofossil Biostratigraphy, Chapman & Hall, London, 16-28, 1998.

Bown, P. R., Lees, J. A., and Young, J. R.: Calcareous nannoplankton evolution and diversity through time, in: Coccolithophores - From Molecular Processes to Global Impact, Springer, Berlin, 481-508, 2004.

Bralower, T..J.: Evidence of surface water oligotrophy during the Paleocene–Eocene thermal maximum: nannofossil assemblage data from Ocean Drilling Program Site 690, Maud Rise, Weddell Sea, Paleoceanography, 17, 1029-1042, doi:10.1029/2001PA000662, 2002.

Bralower,T. J., Mutterlose, J.: Calcareous nannofossil biostratigraphy of ODP Site 865, Allison Guyot, Central Pacific Ocean: a tropical Paleogene reference section. Proc Ocean Drill Prog Sci Results, 143, 31-72, doi:10.2973/odp.proc.sr.143.204.1995, 1995.

Broecker, W. S. and Peng, T.-H.: Tracers in the Sea, Eldigio Press, LamontDoherty Geological Observatory, Palisades, New York, 1-690, 1982.

Buccianti, A., Mateu-Figueras, G., Pawlowsky-Glahn, V.: Compositional data analysis in the geosciences: From theory to practice, Geol. Soc. London, London, Spec. Publ., 264, 1- 12, doi: 10.1144/GSL.SP.2006.264, 2006.Bukry, D.: Low-latitude coccolith biostratigraphic zonation. Initial Rep. Deep Sea Drill. Proj., 15, 685–703, 1973.

Cati, A., Sartorio, D., and Venturini, S.: Carbonate platforms in the subsurface of the northern Adriatic area, Mem. Soc. Geol. It., 40, 295-308, 1989.

Corfield, R. M.: Palaeocene oceans and climate: An isotopic perspective, Earth Sci. Rev., 37, 225-252, doi.org/10.1016/0012-8252(94)90030-2, 1994.

Costa, V., Doglioni, C., Grandesso, P., Masetti, D., Pellegrini, G.B., and Tracanella, E.: Carta Geologica d'Italia, Foglio 063, Belluno: Roma, Servizio Geologico d'Italia, scale 1:50,000, 1 sheet + 74 p., 1996.

Cramer, B. S., Wright, J. D., Kent, D. V., and Aubry, M.-P.: Orbital climate forcing of $\delta^{13}C$ excursions in the late Paleocene– early Eocene (Chrons C24n –C25n), Paleoceanography, 18 (4), 1097, doi:10.1029/2003PA000909, 2003.

Cramer, B. S., Toggweiler, J. R., Wright, J. D., Katz, M. E., and Miller, K. G.: Ocean overturning since the Late Cretaceous: Inferences from a new benthic foraminiferal isotope compilation, Paleoceanogaphy, 24, PA4216, doi:10.1029/2008PA001683, 2009.

Dallanave, E., Agnini, C., Muttoni, G., and Rio, D.: Magneto-biostratigraphy of the Cicogna section (Italy): implications for the late Paleocene-early Eocene time scale, Earth Planet. Sci. Lett., 285, 39-51, doi:10.1016/j.epsl.2009.05.033, 2009.

Dallanave, E., Agnini, C., Bachtadse, V., Muttoni, G., Crampton, J. S., Strong, C. P., Hines, B. R., Hollis, C. J., and Slotnick., B. S.: Early to middle Eocene magnetostratigraphy of the southwest Pacific Ocean and climate influence on sedimentation: insights from the Mead Stream section, New Zealand, Geol. Soc. Am. Bull., 127, 643-660, doi: 10.1130/B31147.1, 2015.

DeConto, R. M., Galeotti, S., Pagani, M., Tracy, D., Schaefer, K. Zhang, T., Pollard, D., and Beerling D. J.: Past extreme warming events linked to massive carbon release from thawing permafrost, Nature, 484, 87-91, doi:10.1038/nature10929, 2012.

Dickens, G. R.: Methane oxidation during the late Palaeocene thermal maximum, Bull. Soc. Geol. France, 171 (1), 37-49, 2000.

Dickens, G. R.: Rethinking the global carbon cycle with a large, dynamic and microbially mediated gas hydrate capacitor, Earth Planet. Sci. Lett., 213, 169-183, 2003.

Dickens, G. R. and Backman, J.: Core alignment and composite depth scale for the lower Paleogene through uppermost Cretaceous interval at Deep Sea Drilling Project Site 577, Newslett. Stratigr., 46, 47-68, doi:10.1127/0078-0421/2013/0027, 2013.

Dickens, G. R., Castillo, M. M., and Walker, J. C. G.: A blast of gas in the latest Paleocene: Simulating first-order effects of massive dissociation of oceanic methane hydrate, Geology, 25, 259–262, 1997.

Doglioni, C. and Bosellini, A.: Eoalpine and mesoalpine tectonics in the Southern Alps, Geol. Rundsch., 77, 734-754, 1987.

Dupuis, C., Aubry, M.-P., Steurbaut, E., Berggren, W.A., Ouda, K., Magioncalda, R., Cramer, B.S., Kent, D.V., Speijer, R.P., and Heilmann-Clausen, C.: The Dababiya Quarry section: lithostratigraphy, geochemistry and paleontology. Micropaleontology, 49 (suppl. 1), 41–59. 2003.

Erba, E., Bottini, C., Weissert, H. J., Keller, C. E.: Calcareous nannoplankton response to surface-water acidification around Oceanic Anoxic Event 1a. Science 329, 428, doi: 10.1126/science.1188886, 2010.

Frank, T. D., Arthur, M. A., and Dean W. E.: Diagenesis of Lower Cretaceous pelagic carbonates, North Atlantic: paleoceanographic signals obscured, J. Foraminiferal Res., 29, 340–351, 1999.

Galeotti, S., Krishnan, S., Pagani, M., Lanci, L., Gaudio, A., Zachos, J. C., Monechi, S., Morelli, G., and Lourens, L.: Orbital chronology of early Eocene hyperthermals from the Contessa Road section, central Italy, Earth Planet. Sci. Lett., 290, 192-200, doi:10.1016/j.epsl.2009.12.021, 2010.

Geisen, M., Young, J. R., Probert, I., Sáez, A. G., Baumann, K.-H., Bollmann, J., Cros, L., De Vargas, C., Medlin, L. K., and Sprengel, C.: Species level variation in coccolithophores, in: Coccolithophores –From Molecular Processes to Global Impact, Springer, Berlin, 327-366, 2004.

Gibbs, S. J., Shackleton, N. J., and Young, J. R.: Orbitally forced climate signals in mid-Pliocene nannofossil assemblages, Mar. Micropaleontol., 51, 39-56, 2004.

Gibbs, S. J., Bown, P. R., Sessa, J. A., Bralower, T. J., and Wilson, P. A.: Nannoplankton extinction and origination across the Paleocene-Eocene thermal maximum, Science, 314, 1770-1773, doi:10.1126/science.1133902, 2006a.

Gibbs, S. J., Bralower, T .J., Bown, P. R., Zachos, J. C., and Bybell, L.M.: Shelf and open-ocean calcareous phytoplankton assemblages across the Paleocene–Eocene thermal maximum: implications for global productivity gradients, Geology, 34, 233-236, doi:10.1130/G22381.1, 2006b.

Gibbs, S. J., Bown, P. R., Murphy, B. H., Sluijs, A., Edgar, K. M., Pälike, H., Bolton, C. T., and Zachos, J.C.: Scaled biotic disruption during early Eocene global warming events, Biogeosciences, 9, 4679-4688, doi:10.5194/bg-9-4679-2012, 2012.

Giusberti, L., Rio, D., Agnini, C., Backman, J., Fornaciari, E., Tateo, F., and Oddone, M.: Mode and tempo of the Paleocene-Eocene Thermal Maximum in an expanded section in the Venetian Pre-Alps, Geol. Soc. Am. Bull., 119, 391-412, doi:10.1130/B25994.1, 2007.

Giusberti, L., Boscolo Galazzo, F., and Thomas, E.: Benthic foraminifera at the Paleocene/Eocene thermal maximum in the western Tethys (Forada section): variability in climate and productivity, Clim. Past Discuss., 11, 4205-4272, doi:10.5194/cpd-11-4205-2015, 2015.Grandesso, P.: Biostratigrafia delle formazioni terziarie del Vallone Bellunese, Boll. Soc. Geol. Ital., 94, 1323-1348, 1976.

Hallock, P.: Fluctuations in the trophic resource continuum: A factor in global diversity cycles?, Paleoceanography, 2, 457–471, 1987.

Hammer, Ø, Harper, D. A. T., and Ryan, P. D.: PAST: Paleontological statistics software package for education and data analysis, Palaeontol. Electron., 4, 9 pp., 2001.

Haq, B. U. and Lohmann, G. P.: Early Cenozoic calcareous nannoplankton biogeography of the Atlantic Ocean, Mar. Micropaleontol., 1, 119-194, 1976.

Harris, A.D., Miller, K.G., Browning, J. V., Sugarman, P.J., Olsson, R.K., Cramer, B.S. and Wright, J.D.;. Integrated stratigraphic studies of Paleocene- lowermost Eocene sequences, New Jersey

Coastal Plain: Evidence for glacioeustatic control. Paleoceanography, 25, PA3211, doi:10.1029/2009PA001800, 2010.Hay, W. W.: Carbonate fluxes and calcareous nannoplankton, in: Coccolithophores - From Molecular Processes to Global Impact, Springer, Berlin, 508-528, 2004.

Hönisch, B., Ridgwell, A., Schmidt, D. N., Thomas, E., Gibbs, S.J., Sluijs, A., Zeebe, R., Kump, L., Martindale, R. C., Greene, S. E., Kiessling, W., Ries, J., Zachos, J. C., Royer, D. L., Barker, S., Marchitto Jr., T. M., Moyer, R., Pelejero, C., Ziveri, P., Foster, G. L., and Williams, B.: The geological record of ocean acidification, Science, 335, 1058-1063, doi:10.1126/science.1208277, 2012.

Hollis, C.J., Taylor, K. W. R., Handley, L., Pancost, R. D., Huber, M., Creech, J. B., Hines, B.R., Crouch, E. M., Morgans, H. E. G., Crampton, J. S., Gibbs, S., Pearson, P. N., and Zachos, J. C.: Early Paleogene temperature history of the southwest Pacific Ocean: Reconciling proxies and models, Earth Planet. Sci. Lett., 349-350, 53-66, 2012.

Huber, M., and Caballero, R.: The Early Eocene equable climate problem revisited, Clim. Past, 7, 603-633, 2011.

Iglesias-Rodriguez, M. D., Halloran, P. R., Rickaby, R. E. M., Hall, I. R., Colmenero-Hidalgo, E., Gittins, J. R., Green, D. R. H., Tyrrell, T., Gibbs, S. J., Von Dassow, P., Rehm, E., Armbrust, E. V., and Boessenkool, K. P.: Phytoplankton calcification in a high-CO_2 world, Science, 320, 336-340, doi:10.1126/science.1154122, 2008.

Jiang, S., and Wise Jr., S.W: Distinguishing the influence of diagenesis on the paleoecological reconstruction of nannoplankton across the Paleocene/Eocene Thermal Maximum: An example from the Kerguelen Plateau, southern Indian Ocean, Mar. Micropaleontol., 72, 49-59, doi: 10.1016/j.marmicro.2009.03.003, 2009.

Keeling, C. D. and Whorf, T. P.: Atmospheric carbon dioxide record from Mauna Loa, in: Oak Ridge Laboratory Trends: A Compendium of Data on Global Change. Carbon Dioxide Information Analysis Center, Oak Ridge National Laboratory, U.S. Department of Energy, Oak Ridge, Tennessee, U.S.A., http://cdiac.esd.ornl.gov/trends/co2/sio-keel-flask/sio-keel-flask.html, 2004.

Kirtland-Turner, S., Sexton, P. F., Charles, C. D., and Norris, R. D.: Persistence of carbon release events through the peak of early Eocene global warmth, Nature Geosci., 7, 748-751, doi:10.1038/ngeo2240, 2014.

Kleypas, J. A., Feely, R. A., Fabry, V. J., Langdon, C., Sabine, C. L., and Robbins, L. L.: Impacts of ocean acidification on coral reefs and other marine calcifiers: A guide for future research, Contrib. No. 2857, NOAA/Pacific Marine Environm. Lab., 88 pp., 2006.

Komar, N., Zeebe, R. E., and Dickens, G.R.: Understanding long-term carbon cycle trends: The late Paleocene through the early Eocene. Paleoceanography, 28, 650-662, doi:10.1002/palo.20060, 2013.

Krishnan, S., Pagani, M., Agnini, C.: Leaf waxes as recorders of paleoclimatic changes during the Paleocene-Eocene Thermal Maximum: Regional expressions from the Belluno Basin. Organic Geochemistry, 80, 8-17, doi: 10.1016/j.orggeochem.2014.12.005, 2015.

Kroopnick, P. M.: The distribution of ^{13}C of ΣCO_2 in the world oceans, Deep Sea Res. Part A, 32, 57-84, 1985.

Kucera, M., Malmgren, B.A.: Logratio transformation of compositional data — a resolution of the constant sum constraint, Mar. Micropaleontol., 34, 117-120, 1998.Kump, L. R., Bralower, T. J., and Ridgwell, A.: Ocean acidification in deep time, Oceanography, 22, 94-107, 2009.

Kurtz, A. C., Kump, L. R., Arthur, M. A., Zachos, J. C., and Paytan, A.: Early Cenozoic decoupling of the global carbon and sulfur cycles, Paleoceanography, 18, 1090, doi:10.1029/2003PA000908, 2003.

Langer, G., M., Geisen, Baumann, K.-H., Kläs, J., Riebesell, U., Thoms, S., and Young, J. R.: Species-specific response of calcifying algae to changing seawater carbonate chemistry, Geochem. Geophys. Geosyst., 7, Q09006, doi:10.1029/2005GC001227, 2006.

Leon-Rodriguez, L. and Dickens, G. R.: Constraints on ocean acidification associated with rapid and massive carbon injections: The early Paleogene record at Ocean Drilling Program Site 1215, Equatorial Pacific Ocean, Palaeogeogr. Palaeoclimatol. Palaeoecol., 298, 409-420, doi:org/10.1016/j.palaeo.2010.10.029, 2010.

Lohbeck, K. T., Riebesell, U., and Reusch, T. B. H.: Adaptive evolution of a key phytoplankton species to ocean acidification, Nature Geosci., 5, 346-351, doi:10.1038/ngeo1441, 2012.

Lourens, L. J., Sluijs, A., Kroon, D., Zachos, J. C., Thomas, E., Röhl, U., Bowles, J., and Raffi, I.: Astronomical pacing of late Palaeocene to early Eocene global warming events, Nature, 435, 1083-1087, doi:10.1038/nature03814, 2005.

Lunt, D. J., Ridgwell, A., Sluijs, A., Zachos, J. C., Hunter, S., and Haywood, A.: A model for orbital pacing of methane hydrate destabilization during the Palaeogene, Nature Geosci., 4, 775-778, doi:10.1038/ngeo1266, 2011.

MacArthur, R. and Wilson, E .O.: The Theory of Island Biogeography, Princeton University Press, ISBN 0-691-08836-5M, 1967.

Marino, M., Maiorano, P., and Lirer, F.: Changes in calcareous nannofossil assemblages during the Mid-Pleistocene Revolution, Mar. Micropaleontol., 69, 70-90, doi:10.1016/j.marmicro.2007.11.010, 2008.

Martini, E.: Standard Tertiary and Quaternary calcareous nannoplankton zonation, in: Proceedings of the 2nd Planktonic Conference, 2, Tecnoscienza, Roma, 739-785, 1971.

Matter, A., Douglas, R. G., and Perch-Nielsen, K: Fossil preservation, geochemistry and diagenesis of pelagic carbonates from Shatsky Rise, northwest Pacific, Init. Rep. DSDP, 32, 891–922, 1975.

Mixon, R.B. and Powars D.S.: Folds and faults in the inner Coastal Plain of Virginia and Maryland: their effect on the distribution and thickness of Tertiary rock units and local geomorphic history. In Frederiksen N.O., and Kraft K. (Eds.), Cretaceous and Tertiary Stratigraphy, paleontology, and structure, southwestern Maryland and northeastern Virginia. American Association of Stratigraphic Palynologists Field Trip Volume and Guidebook (1984), 112–122, 1994

Milliman, J. D.: Production and accumulation of calcium carbonate in the ocean: Budget of a nonsteady state. Global Biogeochemical Cycles, 7, 927-957, doi: 10.1029/93GB02524, 1993.

Monechi, S., Angori, E., von Salis, K.: Calcareous nannofossil turnover around the Paleocene/Eocene transition at Alamedilla (southern Spain). Bull. Soc. Geol. Fr., 171, 477–489, 2000.

Mutterlose, J., Linnert, C., and Norris, R.: Calcareous nannofossils from the Paleocene–Eocene Thermal Maximum of the equatorial Atlantic (ODP Site 1260B): Evidence for tropical warming, Mar. Micropaleontol., 65, 13-31, doi:10.1016/j.marmicro.2007.05.004, 2007.

Nicolo, M. J., Dickens, G. R., Hollis, C. J., and Zachos, J. C.: Multiple early Eocene hyperthermals: Their sedimentary expression on the New Zealand continental margin and in the deep sea, Geology, 35, 699-702, doi:10.1130/G23648A.1, 2007.

Norris, R.D., Wilson, P.A, Blum, P., and the Expedition 342 Scientists: Expedition 342 summary. Proc. IODP, 342, 1-149, doi:10.2204/iodp.proc.342.2014, 2014.

Ogg, J.G., and Bardot, L.: Aptian through Eocene magnetostratigraphic correlation of the Blake Nose Transect (Leg 171B), Florida continental margin, Proc. ODP, Sci. Results, 171B, 1-58, doi:10.2973/odp.proc.sr.171B.104.2001 2001.

Okada, H., and Bukry, D.: Supplementary modification and introduction of code numbers to the low-latitude coccolith biostratigraphic zonation (Bukry, 1973; 1975), Mar. Micropaleontol., 5, 321-325, doi:10.1016/0377-8398(80)90016-X, 1980.

Pälike, H., Lyle, M. W., Nishi, H., Raffi, I., Ridgwell, A., Gamage, K., Klaus, A., Acton, G. D., Anderson, L., Backman, J., Baldauf, J. G., Beltran, C., Bohaty, S. M., Bown, P. R., Busch, W. H., Channell, J. E. T., Chun, C. O. J., Delaney, M. L., Dewang, P., Dunkley Jones, T., Edgar, K. M., Evans, H. F., Fitch, P., Foster, G. L., Gussone, N., Hasegawa, H., Hathorne, E. C., Hayashi, H., Herrle, J. O., Holbourn, A. E. L., Hovan, S. A., Hyeong, K., Iijima, K., Ito, T., Kamikuri, S.-I., Kimoto, K., Kuroda, J., Leon-Rodriguez, L., Malinverno, A., Moore, T. C., Murphy, B., Murphy, D. P., Nakamura, H., Ogane, K., Ohneiser, C., Richter, C., Robinson, R. S., Rohling, E. J., Romero, O. E., Sawada, K., Scher, H. D., Schneider, L., Sluijs, A., Takata, H., Tian, J., Tsujimoto, A., Wade, B. S., Westerhold, T., Wilkens, R. H., Williams, T., Wilson, P. A., Yamamoto, Y., Yamamoto, S., Yamazaki, T., and Zeebe, R. E.: A Cenozoic record of the equatorial Pacific carbonate compensation depth, Nature, 488, 609-614, doi:10.1038/nature11360, 2012

Payros, A., Ortiz, S., Millán, I., Arostegi, J., Orue-Etxebarria, X., and Apellaniz, E.: Early Eocene climatic optimum: Environmental impact on the north Iberian continental margin, Geol. Soc. Am. Bull.,127, 1632-1644doi:10.1130/B31278.1, 2015.

Pearson, P. N., van Dongen, B. E., Nicholas, C. J., Pancost, R. D., Schouten, S., Singano, J. M., and Wade, B. S.: Stable warm tropical climate through the Eocene Epoch, Geology, 35, 211-214, 2007.

Perch-Nielsen, K.: Cenozoic calcareous nannofossils, in: Plankton stratigraphy, Cambridge Univ. Press, New York, 427-554, 1985.

Pianka, E. R.: On r and K selection. Amer. Natural., 104, 592-597, doi:10.1086/282697, 1970.

Premoli Silva, I. and Sliter, W.V.: Cretaceous paleoceanography: Evidence from planktonic foraminiferal evolution, Geol. Soc. Am. Spec. Pap., 332, 301-328, doi:10.1130/0-8137-2332-9.301, 1999.

Raffi, I., Backman, J., and Pälike, H.: Changes in calcareous nannofossil assemblage across the Paleocene/Eocene transition from the paleo-equatorial Pacific Ocean, Palaeogeogr. Palaeoclimatol. Palaeoecol., 226, 93-126, doi:10.1016/j.palaeo.2005.05.006, 2005.

Raffi, I., and De Bernardi, B.: Response of calcareous nannofossils to the Paleocene-Eocene Thermal Maximum: Observations on composition, preservation and calcification in sediments from ODP Site 1263 (Walvis Ridge - SW Atlantic), Mar. Micropaleontol., 69, 119-138, doi: 10.1016/j.marmicro.2008.07.002, 2008.

Raffi, I., Backman, J., Zachos, J.C., Sluijs, A.: The response of calcareous nannofossil assemblages to the Paleocene Eocene Thermal Maximum at the Walvis Ridge in the South Atlantic. Mar. Micropaleontol., 70, 201-212, doi:10.1016/j.marmicro.2008.12.005, 2009.

Riebesell, U., Zondervan, I., Rost, B., Tortell, P. D., Zeebe, R. E., and Morel, F. M. M.: Reduced calcification of marine plankton in response to increased atmospheric CO_2, Nature, 407, 364-367, doi:10.1038/35030078, 2000.

Riebesell, U., Bellerby, R. G. J., Engel, A., Fabry, V. J., Hutchins, D. A., Reusch, K.G., Schulz, T. B. H., and Morel, F. M. M.: Comment on "Phytoplankton calcification in a high-CO2 world", Science, 322, 1466b, doi:10.1126/science.1161096, 2008.

Romein, A.J.T.: Lineages in early Paleogene calcareous nannoplankton. Utrecht Micropaleont. Bull., 22, 1-231, 1979.

Rost, B. and Riebesell, U.: Coccolithophores and the biological pump: responses to environmental changes, in: Coccolithophores - From Molecular Processes to Global Impact, Springer, Berlin, 99-125, 2004.

Roth, P.H.: Jurassic and Lower Cretaceous calcareous nannofossils in the western North Atlantic (Site 534): biostratigraphy, preservation, and some observations on biogeography and paleoceanography, DSDP Init. Repts., 76, 587-621, 1983.

Roth, P.H., and Thierstein, H.R.: Calcareous nannoplankton: Leg XIV of the Deep Sea Drilling Project, DSDP Init. Repts., 14, 421-486, 1972.
Schrag, D.P., DePaolo, D.J., and Richter, F.M.: Reconstructing past sea surface temperatures: correcting for diagenesis of bulk marine carbonate, Geochim. Cosmochim. Acta, 59, 2265-2278, 1995.
Scholle P. A., and Arthur, M. A.: Carbon isotope fluctuations in Cretaceous pelagic limestones: potential stratigraphic and petroleum exploration tool, Amer. Assoc. Pet. Geol. Bulletin, 64, 67-87, 1980.
Self-Trail, J. M., Powars, D. S., Watkins, D. K., and Wandless, G.: Calcareous nannofossil assemblage changes across the Paleocene-Eocene thermal maximum: Evidence from a shelf setting, Mar. Micropaleontol., 92-93, doi:10.1016/j.marmicro.2012.05.003, 2012.
Shackleton, N. J.: Paleogene stable isotope events, Palaeogeogr. Palaeoclimatol. Palaeoecol., 57, 91-102, 1986.
Shamrock, J.L.: Eocene calcareous nannofossil biostratigraphy, paleoecology and biochronology of ODP Leg 122 Hole 762c, Eastern Indian Ocean (Exmouth Plateau). PhD thesis, University of Nebraska, 2010.
Slotnick, B. S., Dickens, G. R., Nicolo, M. J., Hollis, C. J., Crampton, J. S., Zachos, J. C., and Sluijs, A.: Large-amplitude variations in carbon cycling and terrestrial weathering during the latest Paleocene and earliest Eocene: The record at Mead Stream, New Zealand, J. Geol., 120, 1-19, doi:10.1086/666743, 2012.
Slotnick, B. S., Lauretano, V., Backman, J., Dickens, G. R., Sluijs, A., and Lourens, L.: Early Paleogene variations in the calcite compensation depth: new constraints using old borehole sediments from across Ninetyeast Ridge, central Indian Ocean, Clim. Past, 11, 473-493, , doi:10.5194/cp-11-473-2015, 2015a.
Slotnick, B. S., Dickens, G. R., Hollis, C. J., Crampton, J. S., Strong, C. P., and Phillips, A.: The onset of the Early Eocene Climatic Optimum at Branch Stream, Clarence River valley, New Zealand, New Zeal. J. Geol. Geophys., 58, 262-280 doi: 10.1080/00288306.2015.1063514, 2015b.
Spofforth, D. J. A., Agnini, C., Pälike, H., Rio, D., Fornaciari, E., Giusberti, L., Luciani, V., Lanci, L., Muttoni, G., and Bohaty, S. M.: Organic carbon burial following the Middle Eocene Climatic Optimum (MECO) in the central - western Tethys, Paleoceanography, 25, PA3210, doi:10.1029/2009PA001738, 2010.
Stefani, C. and Grandesso, P.: Studio preliminare di due sezioni del Flysch bellunese, Rend. Soc. Geol. It., 14, 157-162, 1991.
Stillman, J. H., and Paganini, A. W., Biogeochemical adaptation to ocean acidifcation, J. Exper. Biology, 218, 1946-1955, doi:10.1242/jeb.115584, 2015.
Stoll, H.M., and Bains, S.: Coccolith Sr/Ca records of productivity during the Paleocene–Eocene thermal maximum from theWeddell Sea. Paleoceanography, 18(2), 1049, doi:10.1029/2002PA000875, 2003.
Tagliabue, A., and L. Bopp: Towards understanding global variability in ocean carbon-13, Global Biogeochem. Cycles, 22, GB1035, doi:10.1029/2007GB003037, 2008.
Thierstein, H. R., Geitzenauer, K. R., Molfino, B., and Shackleton, N. J.: Global synchroneity of late Quaternary coccolith datum levels: validation by oxygen isotopes, Geology, 5, 400-404, 1977.
Thibault, N. and Gardin, S.: The calcareous nannofossil response to the end-Cretaceous warm event in the tropical Pacific, Palaeogeogr. Palaeoclimatol. Palaeoecol., 291, 239-252, doi:10.1016/j.palaeo.2010.02.036, 2010.
Tipple, B. J., Pagani, M., Krishnan, S., Dirghangi, S. S., Galeotti, S., Agnini, C., Giusberti, L., and Rio, D.: Coupled high-resolution marine and terrestrial records of carbon and hydrologic cycles

variations during the Paleocene-Eocene Thermal Maximum (PETM), Earth Planet. Sci. Lett., 311, 82-92, doi:10.1016/j.epsl.2011.08.045, 2011.

Toffanin, F., Agnini, C., Fornaciari, E., Rio, D., Giusberti, L., Luciani, V., Spofforth, D. J. A., and Pälike, H.: Changes in calcareous nannofossil assemblages during the Middle Eocene Climatic Optimum: clues from the central-western Tethys (Alano section, NE Italy), Mar. Micropaleontol., 81, 22-31, doi:10.1016/j.marmicro.2011.07.002, 2011.

Toffanin, F., Agnini, C., Rio, D., Acton, G., and Westerhold, T.: Middle Eocene to early Oligocene calcareous nannofossil biostratigraphy at IODP Site U1333 (equatorial Pacific), Micropaleontol., 59, 69-82, 2013.

Tremolada, F. and Bralower, T. J.: Nannofossil assemblage fluctuations during the Paleocene–Eocene Thermal Maximum at Sites 213 (Indian Ocean) and 401 (North Atlantic Ocean): palaeoceanographic implications, Mar. Micropaleontol., 52, 107-116, doi:10.1016/j.marmicro.2004.04.002, 2004.

Vandenberghe, N., Hilgen, F. J., and Speijer, R. P.: The Paleogene Period, in: The Geologic Time Scale 2012, Amsterdam, the Netherlands (Elsevier BV), 855–922, 2012.

Watkins, D. K. and Self-Trail, J. M.: Calcareous nannofossil evidence for the existence of the Gulf Stream during the late Maastrichtian, Paleoceanography, 20, Pa3006, doi:10.1029/2004pa001121, 1992.

Wei, W., and Wise Jr. S. W.: Biogeographic gradients of middle Eocene–Oligocene calcareous nannoplankton in the South Atlantic Ocean, Palaeogeogr. Palaeoclimatol. Palaeoecol., 79, 29-61, 1990.

Westerhold, T., Röhl, U., Raffi, I., Fornaciari, E., Monechi, S., Reale, V., Bowles, J., and Evans, H. F.: Astronomical calibration of the Paleocene time, Palaeogeogr. Palaeoclimatol. Palaeoecol., 257, 377-403, doi:10.1016/j.palaeo.2007.09.016, 2008.

Westerhold, T., Röhl, U., Donner, B., McCarren, H.K. and Zachos, J.C.: A complete high - resolution Paleocene benthic stable isotope record for the central Pacific (ODP Site 1209). Paleoceanography, 26, PA2216,doi:10.1029/2010PA002092, 2011

Winter, A., Jordan, R.W., and Roth, P.H.: Biogeography of living coccolithophores. in: Coccolithophores edited by Winter, A., and Siesser, W.G., Cambridge Univ. Press, Cambridge , 161-177, 1994.

Winterer, E. L. and Bosellini, A.: Subsidence and sedimentation on Jurassic passive continental margin, Southern Alps, Italy, Am. Assoc. Petr. Geol. Bull., 65, 394-421, 1981.

Young, J. R., Geisen, M., and Probert, I.: A review of selected aspects of coccolithophore biology with implications for paleobiodiversity estimation, Micropaleontology, 51, 267-288, 2005.,

Zachos, J.C., Kroon, D., Blum, P., et al.: Early Cenozoic Extreme Climates: The Walvis Ridge Transect. Proc. Ocean Drill. Program, Initial Rep. 208 doi:10.2973/odp.proc.ir.208.2004, 2004.

Zachos, J. C., Röhl, U., Schellenberg, S. A., Sluijs, A., Hodell, D. A., Kelly, D. C., Thomas, E., Nicolo, M., Raffi, I., Lourens, L. J., McCarren, H., and Kroon, D.: Rapid acidification of the ocean during the Paleocene-Eocene Thermal Maximum, Science 308, 1611-1615, doi:10.1126/science.1109004, 2005.

Zachos, J. C., Dickens, G. R., and Zeebe, R. E.: An early Cenozoic perspective on greenhouse warming and carbon-cycle dynamics, Nature, 451, 279-283, doi:10.1038/nature06588, 2008.

Zachos, J. C., McCarren, H., Murphy, B., Röhl, U., and Westerhold, T.: Tempo and scale of late Paleocene and early Eocene carbon isotope cycles: Implications for the origin of hyperthermals. Earth Planet. Sci. Lett., 299, 242-249, doi:10.1016/j.epsl.2010.09.004, 2010.

Zattin, M., Cuman, A., Fantoni, R., Martin, S., Scotti, P., and Stefani, C.: From middle Jurassic heating to Neogene cooling: The thermochronological evolution of the southern Alps, Tectonophysics, 414, 191-202, doi:10.1016/j.tecto.2005.10.020, 2006.

Zeebe, R. E. and Westbroek, P.: A simple model for the $CaCO_3$ saturation state of the ocean: The "Strangelove", the "Neritan", and the "Cretan" ocean, Geochem. Geophys. Geosyst., 4, 1104, doi:10.1029/2003GC000538, 2003, 2003.

Zeebe, R. E., Zachos, J. C., and Dickens, G. R.: Carbon dioxide forcing alone insufficient to explain Paleocene-Eocene Thermal Maximum warming, Nature Geosci., 2, 576-580, doi:10.1038/NGEO578, 2009.

Ziveri, P., Young, J., and van Hinte J. E.: Coccolithophore export production and accumulation rates. in: On determination of sediment accumulation rates, GeoResearch Forum, Trans Tech Publications LTD, Switzerland, 5, 41-56, 1999.

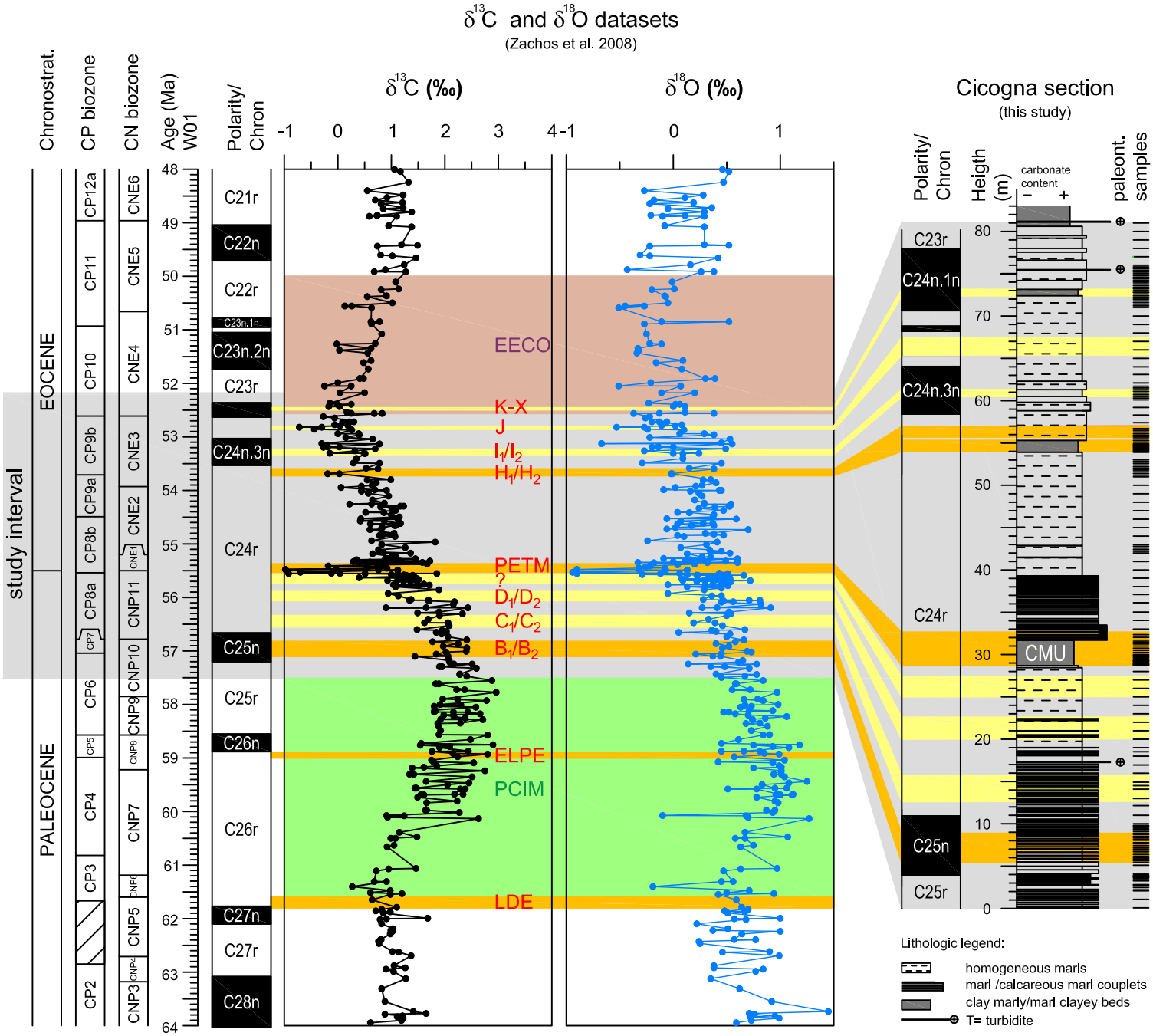

Figure 1_ Agnini et al.

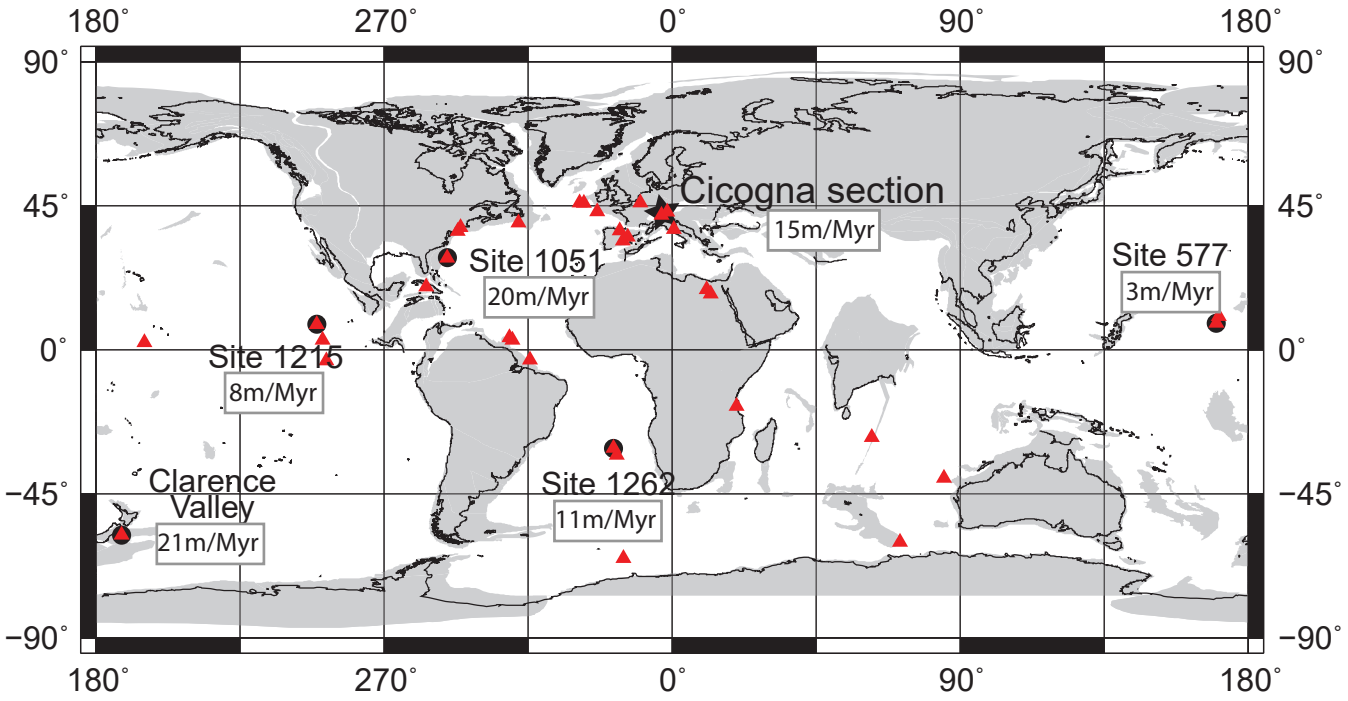

Figure 2_Agnini et al.

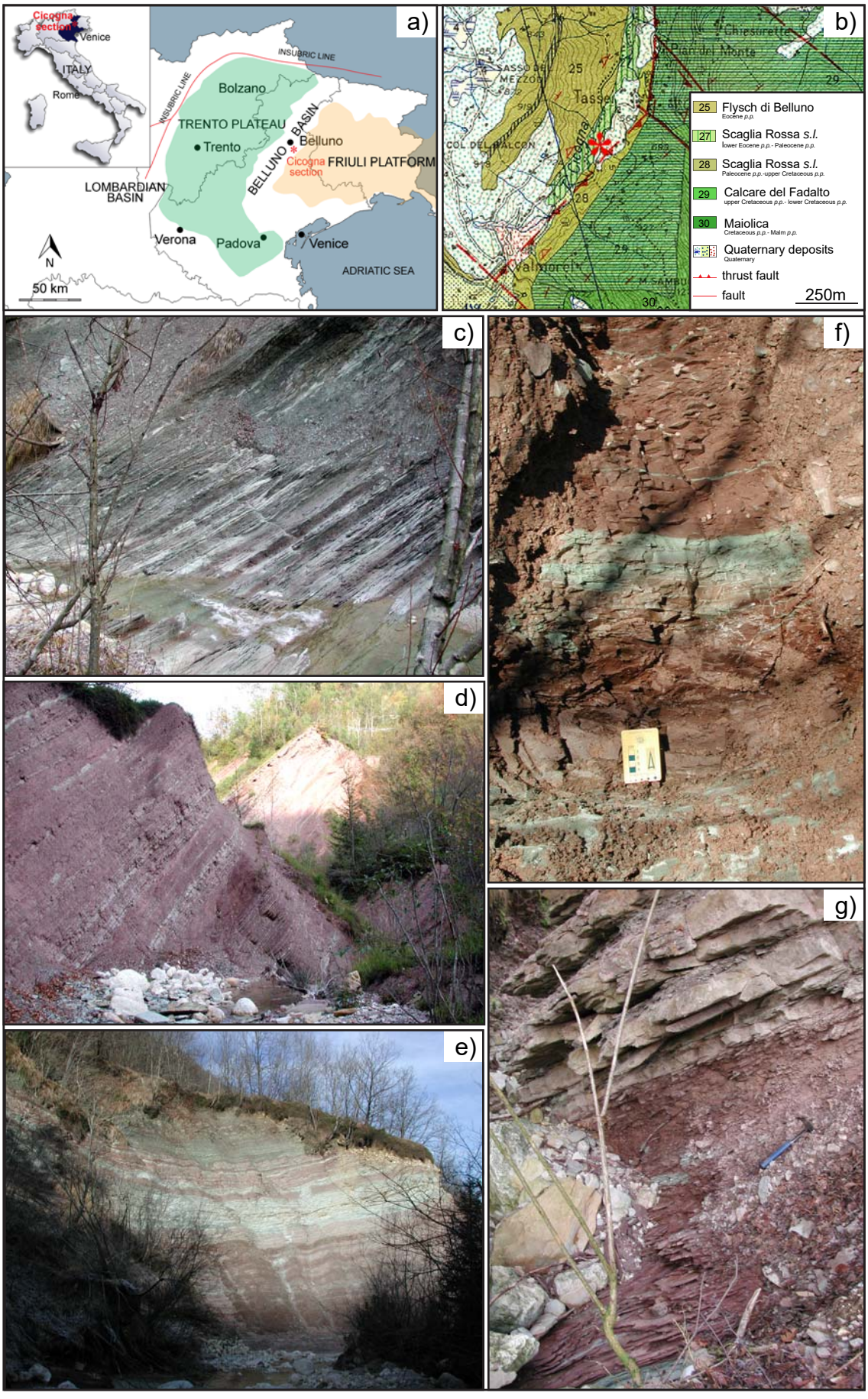

Figure 3_Agnini et al.

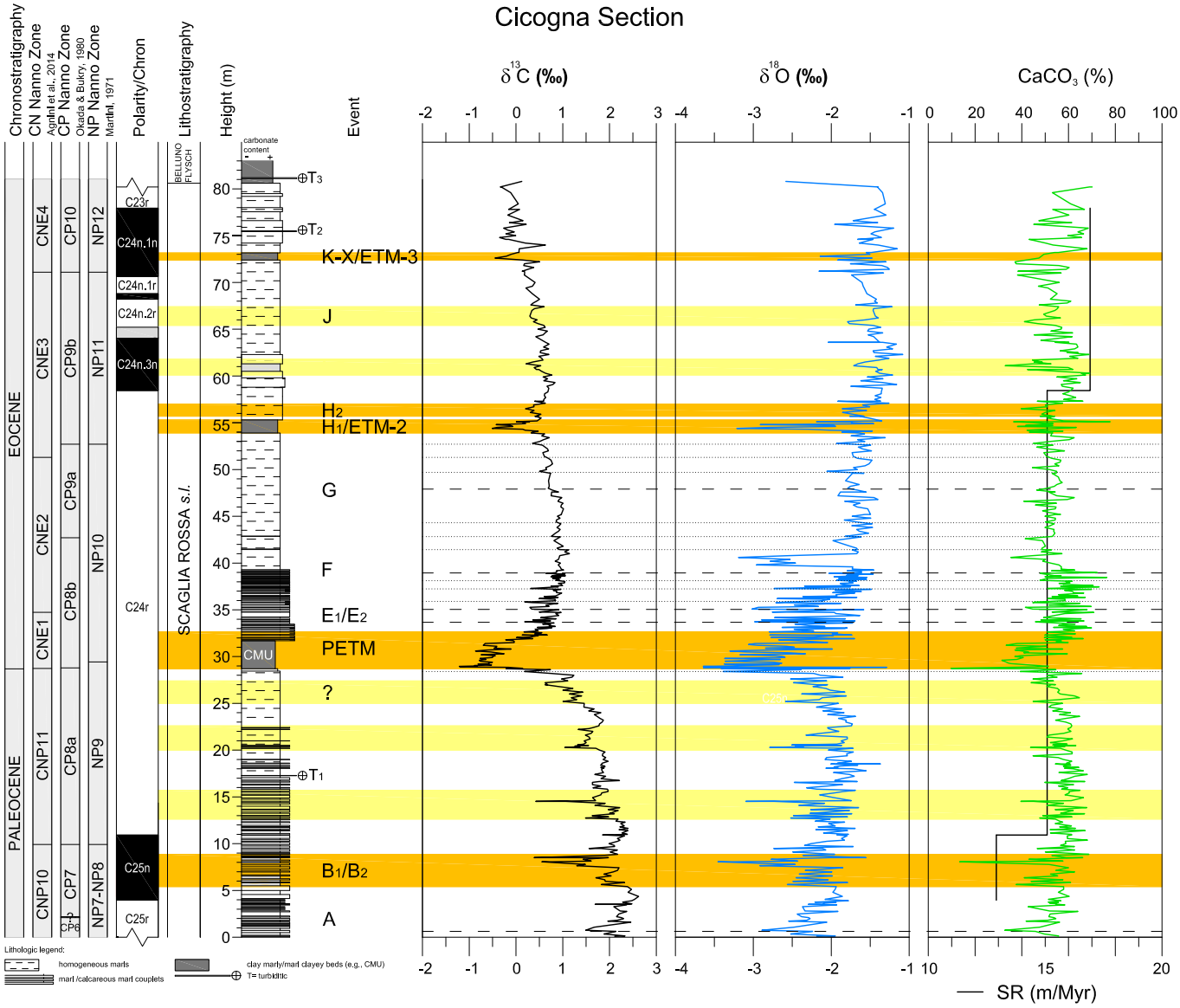

Figure 4_Agnini et al

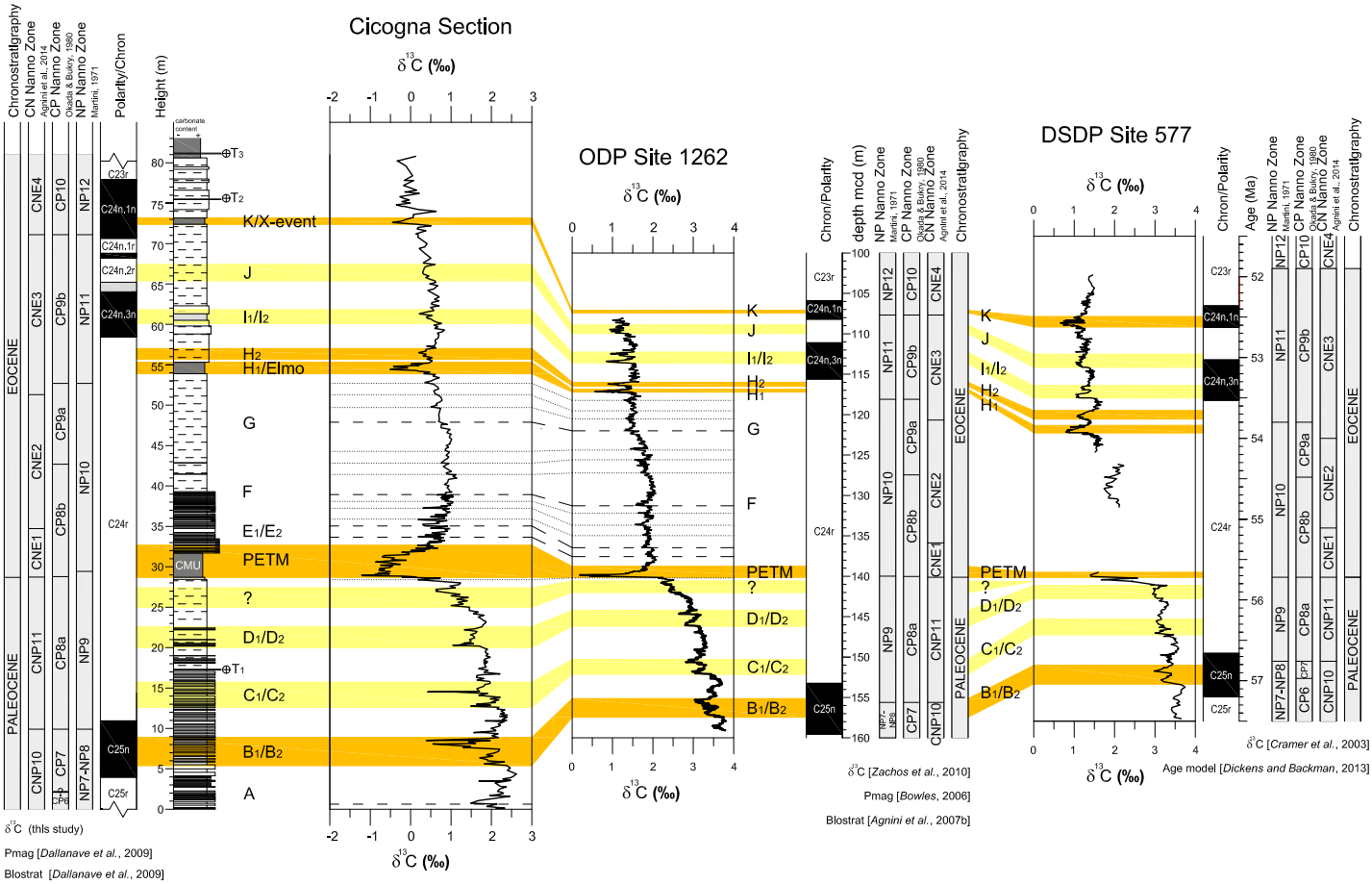

Figure 5_ Agnini et al.

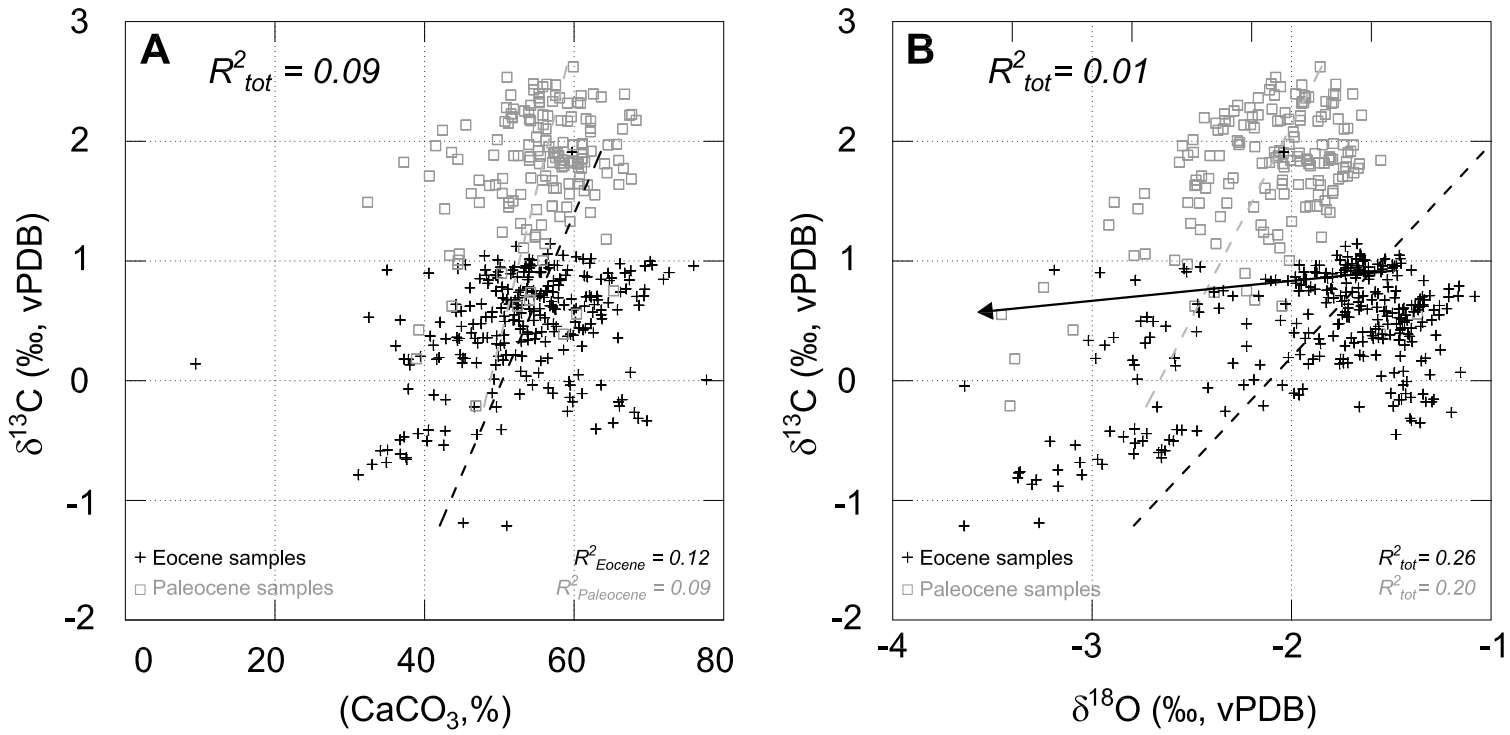

Figure 6_Agnini et al.

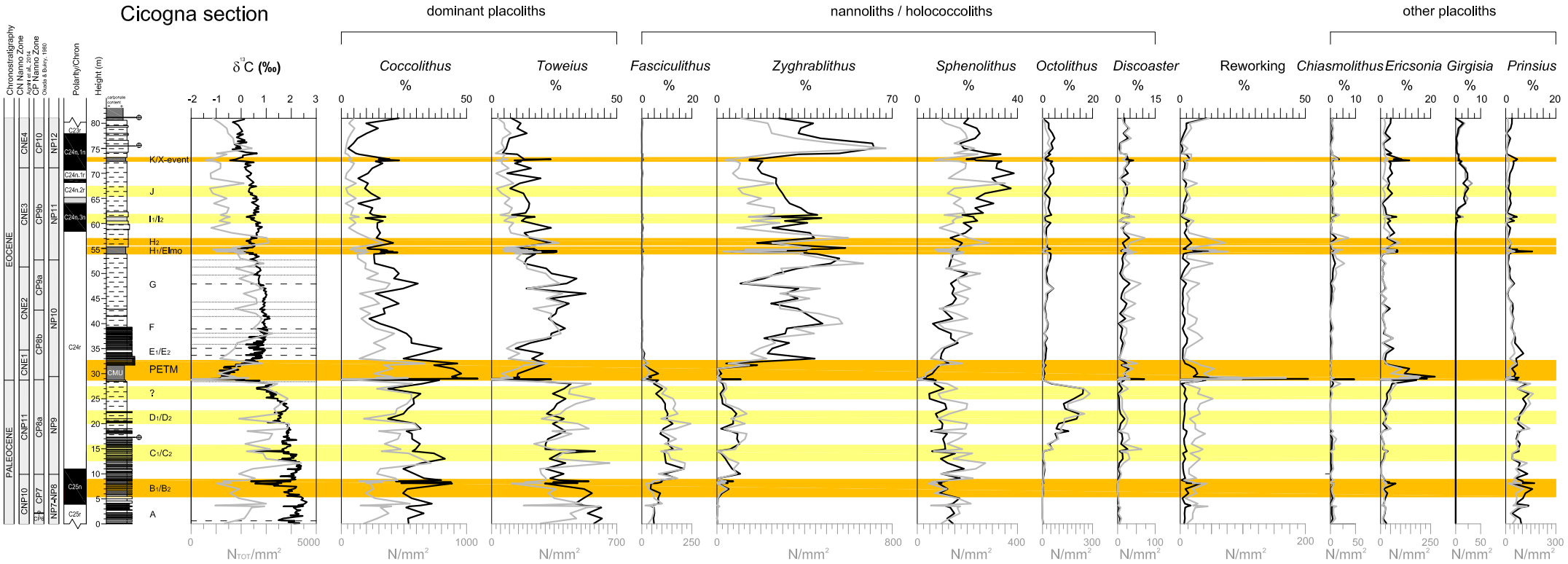

Figure 7_Agnini et al.

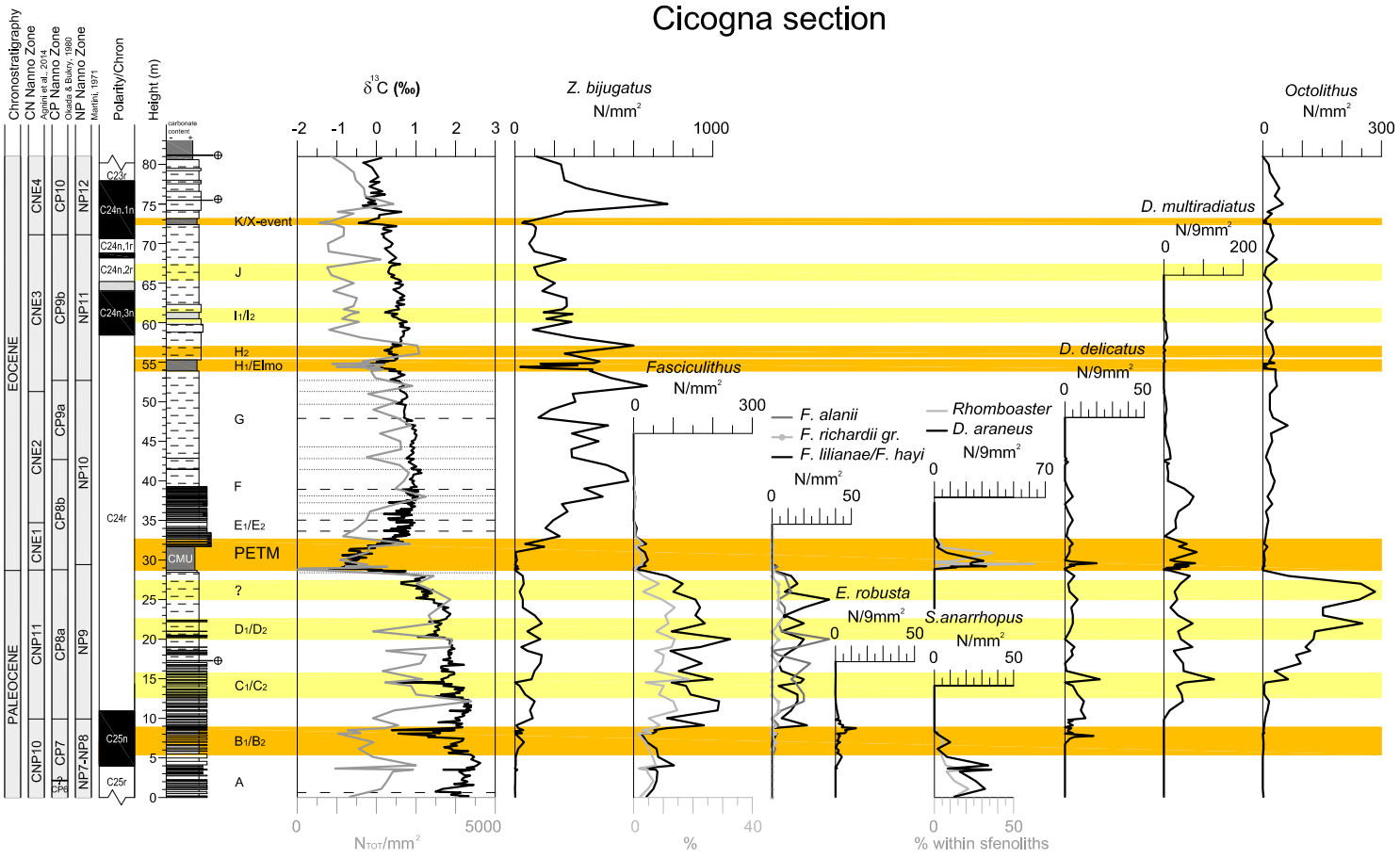

Figure 8_Agnini et al.

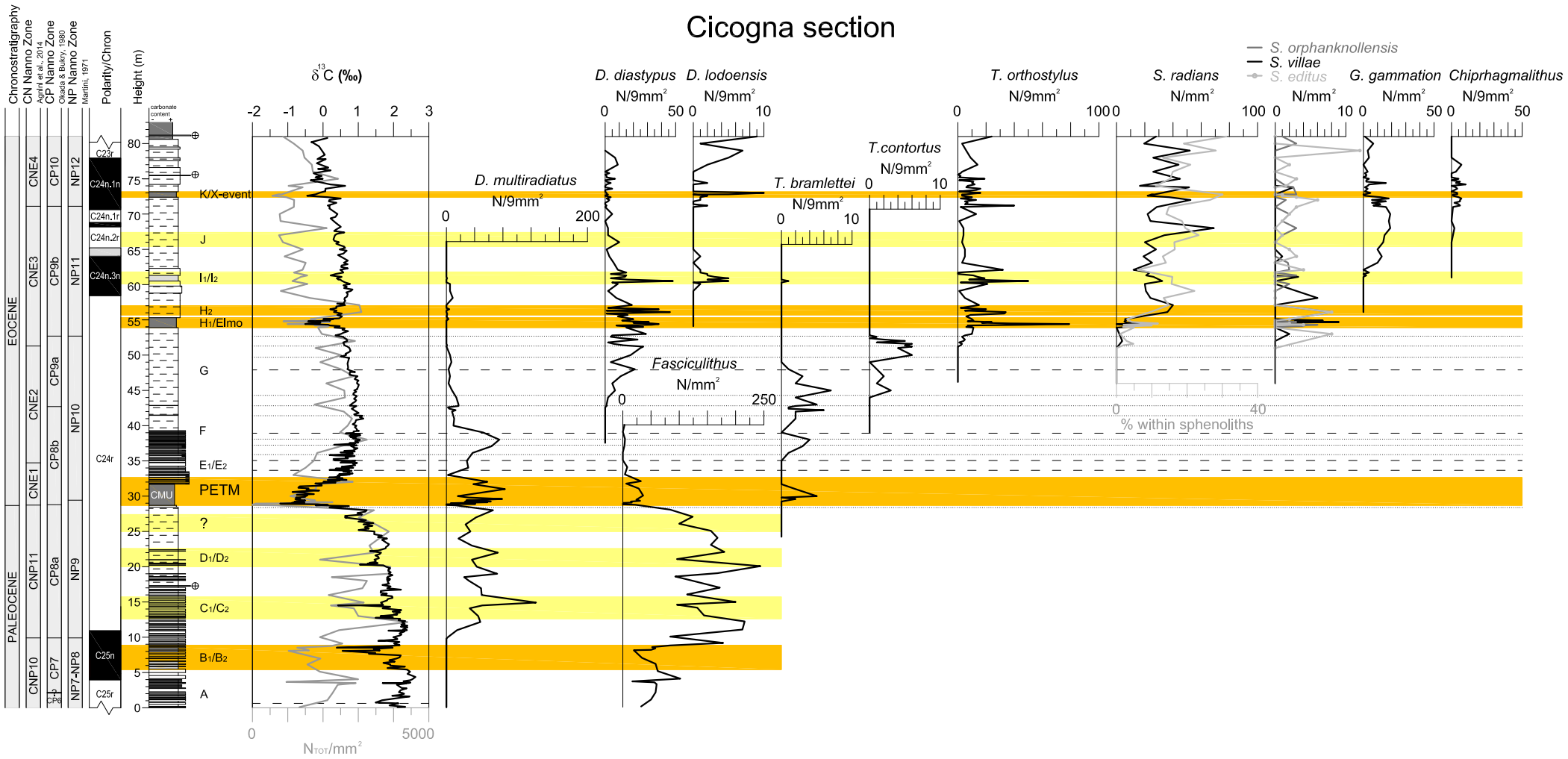

Figure9_Agnini et al.

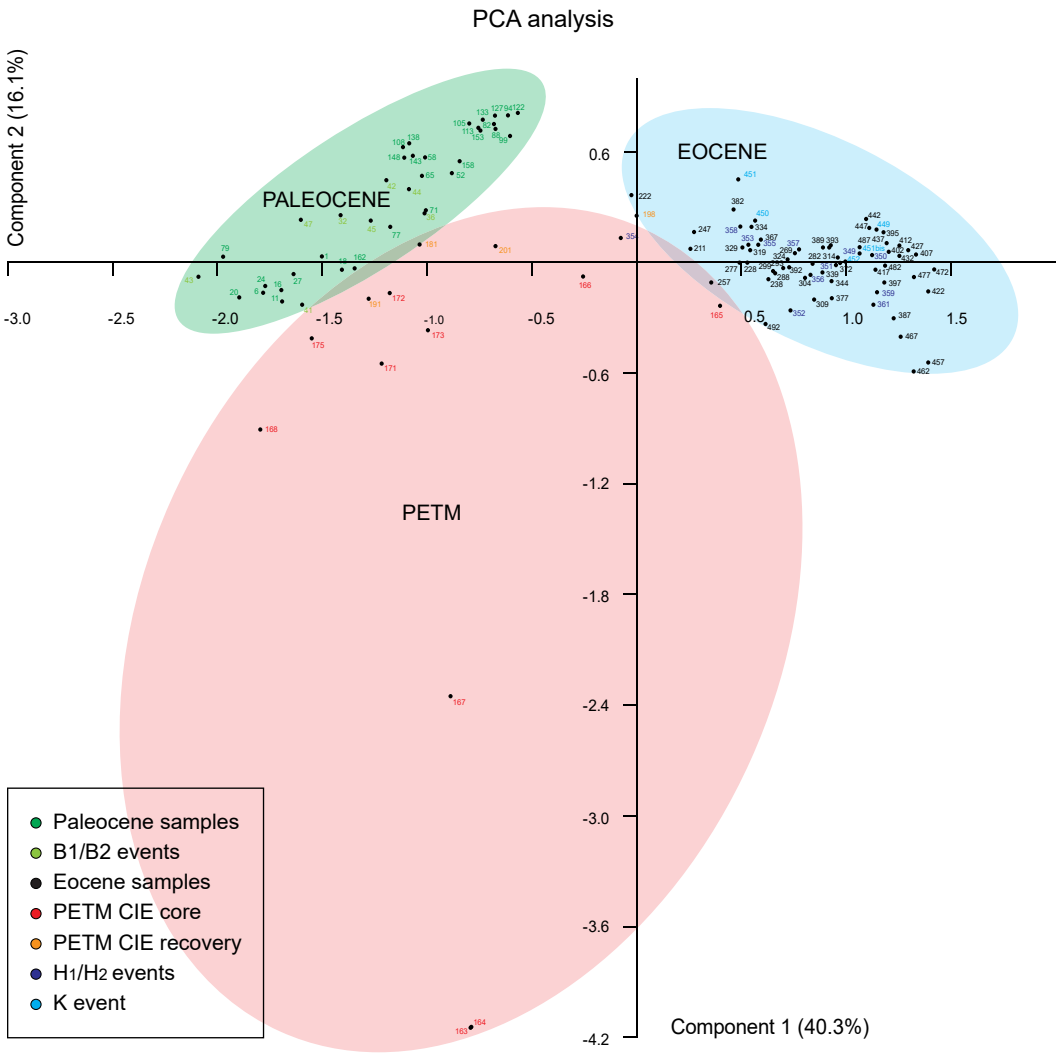

Figure 10_Agnini et al.

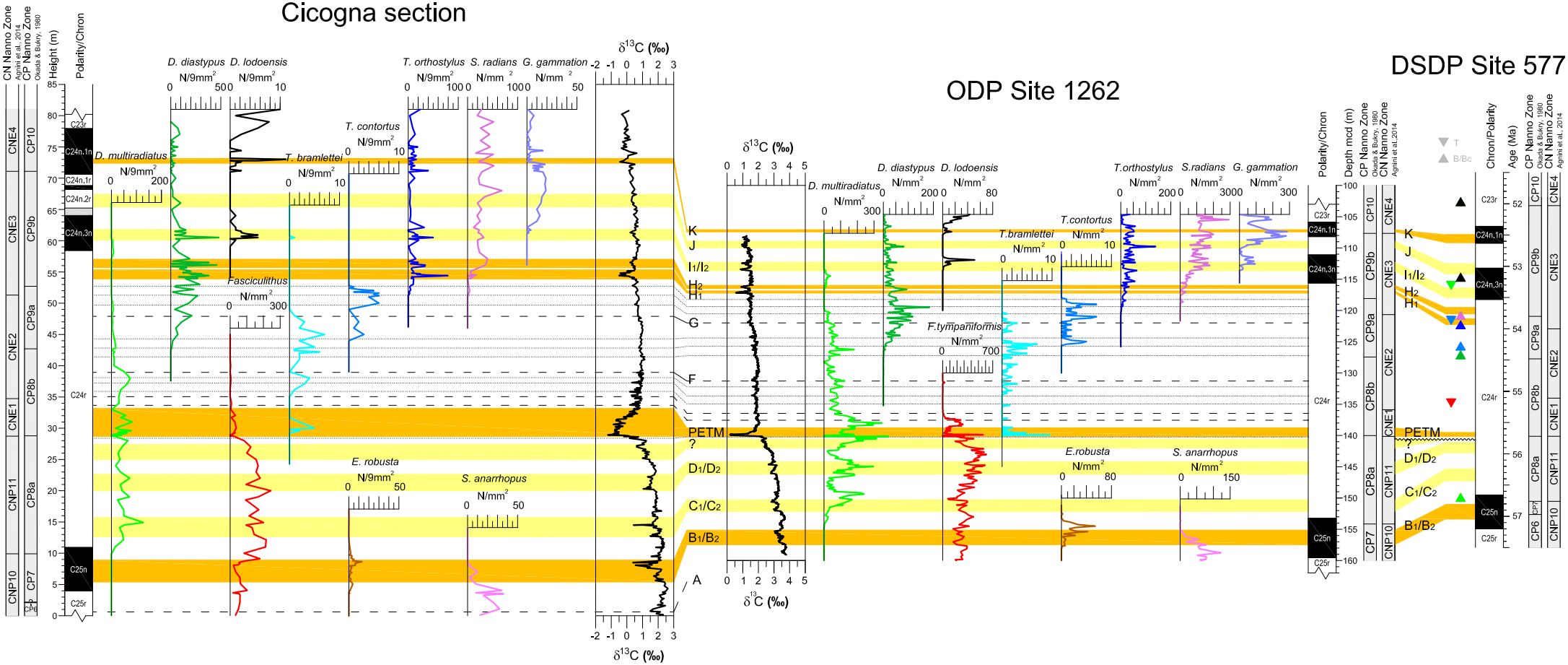

Figure 11_ Agnini et al.

Table 1

Event		Nanno Zones			Cicogna section		DAMR09I		W01	CK95	GTS04	GTS12	Site 1262		AG07+/This study		W01	CK95	GTS04	GTS12
		NP*	CP^	CN°	Height (m)	Err (m)	Chron notation		Age (Ma)	Age (Ma)	Age (Ma)	Age (Ma)	Depth (mcd)	Err (m)	Chron notation		Age (Ma)	Age (Ma)	Age (Ma)	Age (Ma)
	C23r base				77.94				0.000	52.364	52.364	52.648	52.620	105.88			0.000	52.364	52.364	52.648	52.620
	K-X base				72.20	0.10	C24n.1n		0.786	52.57	52.60	52.93	52.98	-	-	-	-	-	-	-	-
B	*Discoaster lodoen*	NP12	CP10		71.10	0.10	C24n.1n		0.936	52.61	52.64	52.98	53.05	107.67	0.18	C24n.1n	0.777	52.57	52.60	52.92	52.97
Bc	*Chiprhagmalithus spp.*				71.10	0.10	C24n.1n		0.936	52.61	52.64	52.98	53.05	107.67	0.18	C24n.1n	0.777	52.57	52.60	52.92	52.97
	C24n.1n base				70.64				0.000	52.630	52.663	53.004	53.074	108.19			0.000	52.630	52.663	53.004	53.074
	C24n.1r base				68.80				0.000	-	52.757	53.116	53.199	-			0.000	-	52.757	53.116	53.199
	C24n.2n base				68.21				0.000	-	52.801	53.167	53.274	-			0.000	-	52.801	53.167	53.274
B	*Chiprhagmalithus spp.*				66.50	0.50	C24n.2r		0.473	52.82	52.85	53.22	53.34	109.22	0.10	C24n.2r/.1r	0.358	52.77	52.75	53.11	53.20
	J base				65.40	0.10	C24n.2r		0.778	52.94	52.88	53.26	53.38	109.96	0.02	C24n.2r/.1r	0.616	52.88	52.81	53.18	53.28
	C24n.2r base				64.60				0.000	53.030	52.903	53.286	53.416	111.06			0.000	53.03	52.903	53.286	53.416
B	*Girgisia gammation*				61.20	0.10	C24n.3n		0.526	53.29	53.14	53.56	53.71	113.52	0.11	C24n.3n	0.540	53.30	53.14	53.57	53.72
Br	*Discoaster lodoensis*				60.40	0.10	C24n.3n		0.650	53.36	53.19	53.63	53.78	113.52	0.11	C24n.3n	0.540	53.30	53.14	53.57	53.72
T	*Discoaster multiradiatus*				60.20	0.10	C24n.3n		0.681	53.37	53.21	53.64	53.80	113.52	0.11	C24n.3n	0.540	53.30	53.14	53.57	53.72
	I1/I2 base				60.10	0.10	C24n.3n		0.697	53.38	53.21	53.65	53.81	113.66	0.02	C24n.3n	0.570	53.32	53.16	53.58	53.74
	C24n.3n base				58.14				0.000	55.530	53.347	53.808	53.983	115.61			0.000	53.530	53.347	53.808	53.983
	H1-Elmo/H2 base				53.90	0.10	C24r		0.090	53.81	53.58	54.06	54.26	117.21	0.01	C24r	0.042	53.66	53.46	53.93	57.12
T	*Tribrachiatus cont*	NP11	CP9b		52.70	0.10	C24r		0.115	53.89	53.64	54.14	54.34	118.09	0.10	C24r	0.066	53.74	53.52	54.00	57.14
Tc	*Discoaster multiradiatus*				51.50	0.10	C24r		0.141	53.97	53.71	54.21	54.42	119.38	0.11	C24r	0.100	53.84	53.60	54.09	57.16
B	*Sphenolithus radians*				51.30	0.10	C24r		0.145	53.98	53.72	54.22	54.43	118.72	0.10	C24r	0.083	53.79	53.56	54.04	57.15
B	*Tribrachiatus orthostylus*			CNE3	51.30	0.10	C24r		0.145	53.98	53.72	54.22	54.43	120.67	0.10	C24r	0.134	53.95	53.69	54.19	57.18
T	*Tribrachiatus bramlettei*				48.50	0.50	C24r		0.204	54.17	53.87	54.39	54.62	121.30	0.11	C24r	0.151	54.00	53.73	54.24	57.18
B	*Tribrachiatus contortus*		CP9a		45.50	0.50	C24r		0.268	54.37	54.03	54.57	54.82	125.50	0.10	C24r	0.263	54.35	54.02	54.56	57.25
B	*Discoaster diastypus*		CP9a		42.70	0.10	C24r		0.327	54.55	54.18	54.74	55.00	127.45	0.10	C24r	0.314	54.51	54.15	54.71	57.28
B	*Tribrachiatus bran*	NP10			35.58	0.55	C24r		0.478	55.03	54.57	55.17	55.47	133.34	0.11	C24r	0.471	55.00	54.55	55.15	57.36
T	*Fasciculithus spp./F. tympaniformis*			CNE2	34.73	0.13	C24r		0.496	55.08	54.61	55.22	55.53	135.87	0.11	C24r	0.538	55.21	54.72	55.35	57.40
T	*Rhomboaster spp.*				32.52	0.48	C24r		0.543	55.23	54.73	55.36	55.67	139.72	0.01	C24r	0.640	55.53	54.98	55.64	57.46
X	*Fasciculithus / Zygrhablithus*				31.60	0.10	C24r		0.562	55.29	54.78	55.41	55.74	139.80	0.02	C24r	0.643	55.54	54.99	55.64	57.46
Br	*Tribrachiatus bramlettei*				29.43	0.18	C24r		0.608	55.43	54.90	55.55	55.88	139.99	0.02	C24r	0.648	55.56	55.00	55.66	57.46
B	*Discoaster araneus*				28.95	0.05	C24r		0.618	55.47	54.93	55.57	55.91	-	-	-	-	-	-	-	-
B	*Rhomboaster spp.*	NP9b	CP8b		28.88	0.03	C24r		0.620	55.47	54.93	55.58	55.92	140.02	0.01	C24r	0.648	55.56	55.01	55.66	57.46
	PETM				28.73	0.03	C24r		0.623	55.48	54.94	55.59	55.93	140.13	0.02	C24r	0.652	55.57	55.01	55.67	57.46
	P/E boundary (extrapolated)				28.73	0.03	C24r		0.623	55.48	54.94	55.59	55.93	140.13	0.02	C24r	0.652	55.57	55.01	55.67	57.46
decrease	*Fasciculithus spp.*				28.73	0.03	C24r		0.623	55.48	54.94	55.59	55.93	140.13	0.02	C24r	0.652	55.57	55.01	55.67	57.46
T	*F. richardii gr.*			CNE1	28.73	0.03	C24r		0.623	55.48	54.94	55.59	55.93	140.13	0.02	C24r	0.652	55.57	55.01	55.67	57.46
	? base				25.00	0.10	C24r		0.702	55.73	55.14	55.81	56.17	142.00	0.02	C24r	0.701	55.72	55.14	55.81	57.49
	D1/D2 base				20.00	0.10	C24r		0.808	56.06	55.41	56.12	56.50	146.17	0.02	C24r	0.812	56.07	55.42	56.13	57.55
	C1/C2 base				12.61	0.10	C24r		0.964	56.55	55.81	56.56	56.99	152.08	0.02	C24r	0.969	56.56	55.82	56.58	57.64
T	*Ericsonia robusta*				11.2	0.2	C24r		0.994	56.64	55.89	56.65	57.08	153.32	0.10	C25n	0.011	56.67	55.91	56.67	57.11
	C24r base				10.93				0.000	56.660	55.904	56.665	57.101	153.25			0.000	56.660	55.904	56.665	57.101
Bc	*F. alanii*				10.51	0.49	C25n		0.060	56.69	55.93	56.70	57.13	152.77	0.02	C24r	0.987	56.62	55.87	56.63	57.65
B	*Discoaster multira*	NP9a			9.90	0.10	C25n		0.147	56.74	55.98	56.74	57.18	154.61	0.11	C25n	0.216	56.78	56.01	56.78	57.22
Tc	*Sphenolithus anarrhopus*				8.62	0.49	C25n		0.331	56.84	56.07	56.84	57.28	155.03	0.11	C25n	0.283	56.81	56.04	56.81	57.26
B	*Discoaster delicatus gr.*				6.86	0.12	C25n		0.583	56.97	56.19	56.97	57.42	156.92	0.11	C25n	0.583	56.97	56.19	56.97	57.42
	B1/B2 base				5.41	0.10	C25n		0.791	57.08	56.29	57.07	57.54	158.37	0.02	C25n	0.813	57.10	56.30	57.08	56.52
B	*Ericsonia robusta*				3.97	0.07	C25n		0.998	57.20	56.39	57.18	57.65	158.00	0.11	C25n	0.754	57.06	56.27	57.05	57.52
	C25n base				3.96				0.000	57.197	56.391	57.180	57.656	159.55			0.000	57.197	56.391	57.180	57.656
B	*Discoaster nobilis gr.*		CP7		2.14	0.05	C25r			57.337	56.518	57.314	57.801	157.35	0.10	C25n	0.651	57.01	56.22	57.00	57.46
B	*D. mohleri*	NP7	CP6		-	-	-		-	-	-	-	-	171.50	0.11	C25r	0.984	58.53	58.53	58.53	58.53
	C25r base				-				0.000	58.550	57.554	58.379	58.959	171.70			0.000	58.550	57.554	58.379	58.959

Reference calcareous nannofossill biozonations: *NP (Martini, 1971); ^CP (Okada and Bukry, 1980); ° CN (Agnini et al., 2014)

Reference timescales: W01 (Westerhold et al., 2008- option1); CK95 (Cande and Kent, 1995); GTS04 (Ogg and Smith, 2004); GTS12 (Ogg, 2012)

IDARM09 (Dallanave et al., 2009)

+AG07 (Agnini et al., 2007)